

# Imprints of Dark Energy on Cosmic Structure Formation

## I) Realistic Quintessence Models and the Non-Linear Matter Power Spectrum

J.-M. Alimi<sup>1,2\*</sup>, A. Füzfa<sup>1,2,3†</sup>, V. Boucher<sup>3‡</sup>, Y. Rasera<sup>1§</sup>, J. Courtin<sup>1¶</sup>, P.-S. Corasaniti<sup>1||</sup>

<sup>1</sup>CNRS, Laboratoire Univers et Théories (LUTH), UMR 8102 CNRS, Observatoire de Paris,  
Université Paris Diderot ; 5 Place Jules Janssen, F-92190 Meudon, France

<sup>2</sup>Groupe d'Application des MATHématiques aux Sciences du COSmos (GAMASCO),  
University of Namur (FUNDP), 61 rue de Bruxelles, B-5000 Namur, Belgium

<sup>3</sup>Center for Particle Physics and Phenomenology (CP3),  
Université catholique de Louvain, 2 Chemin du Cyclotron, B-1348 Louvain-la-Neuve, Belgium

### ABSTRACT

Quintessence has been proposed to account for dark energy in the Universe. This component causes a typical modification of the background cosmic expansion, which in addition to its clustering properties, can leave a potentially distinctive signature on large scale structures. Many previous studies have investigated this topic, particularly in relation to the non-linear regime of structure formation. However, no careful pre-selection of viable quintessence models with high precision cosmological data was performed. Here we show that this has led to a misinterpretation (and underestimation) of the imprint of quintessence on the distribution of large scale structures. To this purpose we perform a likelihood analysis of the combined Supernova Ia UNION dataset and WMAP5-years data to identify realistic quintessence models. These are specified by different model parameter values, but still statistically indistinguishable from the vanilla  $\Lambda$ CDM. Differences are especially manifest in the predicted amplitude and shape of the linear matter power spectrum, though these remain within the uncertainties of the SDSS data. We use these models as benchmark for studying the clustering properties of dark matter halos by performing a series of high resolution N-body simulations. In this first paper, we specifically focus on the non-linear matter power spectrum. We find that realistic quintessence models allow for relevant differences of the dark matter distribution with the respect to the  $\Lambda$ CDM scenario well into the non-linear regime, with deviations up to 40% in the non-linear power spectrum. Such differences are shown to depend on the nature of DE, as well as the scale and epoch considered. At small scales ( $k \sim 1 - 5 \text{ h Mpc}^{-1}$ , depending on the redshift) the structure formation process is about 20% more efficient than in  $\Lambda$ CDM. We show that these imprints are a specific record of the cosmic structure formation history in dark energy cosmologies and therefore cannot be accounted in standard fitting functions of the non-linear matter power spectrum.

**Key words:** cosmology: cosmic microwave background, supernovae, cosmological parameters, dark matter, dark energy, quintessence, large-scale structures of Universe, methods: N-body simulations

\* email: jean-michel.alimi@obspm.fr

† email: andre.fuzfa@fundp.ac.be

‡ email: vincent.boucher@uclouvain.be

§ email: yann.rasera@obspm.fr

¶ email: jerome.courtin@obspm.fr

|| email: pier-stefano.corasaniti@obspm.fr

## 1 INTRODUCTION

Over the past decade cosmological observations have provided mounting evidence in favour of an unexpected energy component — dark energy (DE) — which dominates the present energy content of the Universe and is responsible for the recent cosmic accelerated expansion. Early measurements of the Supernova Ia Hubble diagram (Riess et al. 1998, 2001; Perlmutter et al. 1999) which have been recently confirmed by more accurate detections (Knop et al. 2003; Astier et al. 2006; Riess et al. 2007), in combination with precise measurements of Cosmic Microwave Background (CMB) anisotropies (De Bernardis et al. 2000; Spergel et al. 2003, 2006; Bennett et al. 2003; Komatsu et al. 2008), mapping of the distribution of large scale structures from galaxy survey (Efsthathiou et al. 2002; Tegmark et al. 2004, 2006; Cole et al. 2005; Eisenstein et al. 2005), CMB–Large Scale Structure (LSS) correlation (see Cabre et al. 2006, Giannantonio et al. 2008, McEwen et al. 2008 and references therein), galaxy clusters (Allen, Schmidt & Fabian 2002), peculiar velocities (Mohayaee & Tully 2005) and galaxy redshift distortions (Guzzo et al. 2008) have pinned down the cosmic abundance of the various matter energy components. These data indicate that pressureless matter (baryons and cold dark matter) accounts for only 25% of the total energy content in the Universe, leaving the remaining 75% to be dark energy.

In light of these observations the existence of DE phenomenon can hardly be contested nowadays, thus the question of its physical origin has become crucial especially from a fundamental physics perspective. The simplest scenario to account for a late time cosmic acceleration consists of a positive cosmological constant  $\Lambda$  in Einstein’s equations of general relativity. Nevertheless, the fact that today  $\rho_\Lambda$  is of the order of the matter density  $\rho_m$  suggests that we are living in a period of remarkable coincidence, since the value of  $\Lambda$  must have been fixed very precisely at early times as to allow for a sufficient period of structure formation responsible for the distribution of matter that we observe today (see e.g. Weinberg 1989). One can hope that understanding the physical nature of  $\Lambda$  may solve this puzzling coincidence, but all known attempts have led to an even more troubling problem that can be explained only if an anthropic selection mechanism is at work. In fact the cosmological constant can be naturally interpreted as the energy contribution of quantum vacuum fluctuations, however Standard Model fields give rise to a vacuum energy density up to 119 order of magnitudes (assuming a cut-off at the Planck scale) larger than the cosmological constant observed value, hence requiring an unnatural fine-tuning of the bare cosmological constant such as to ensure a precise cancellation of the energy associated to quantum vacuum diagrams. We still lack of a convincing theoretical explanation for this naturalness problem, and it may well be that the dark energy phenomenon is of complete different origin.

Several scenarios have been proposed in a vast literature, which include the existence of a light minimally coupled scalar field dubbed *quintessence* (Wetterich 1988; Ratra & Peebles 1988) motivated by physics beyond the Standard Model of particle physics, deviations from standard general relativity on cosmological scales due to higher order corrections to Einstein gravity (see e.g. Capozziello, Cardone & Troisi 2005), and modifications due to the presence of extra dimensions (Dvali, Gabadadze and Porrati 2000). In quintessence cosmologies the late time dynamics of the scalar field is responsible for driving the cosmic accelerated expansion (see Copeland, Sami & Tsujikawa 2006 for a review). As the field rolls down its self-interaction potential the kinetic energy becomes small compared to the potential energy, causing the field pressure becoming sufficiently negative such as to drive the acceleration, namely  $w_{DE} = p_{DE}/\rho_{DE} < -1/(3\Omega_{DE})$  (for a flat universe) at present time, where  $\Omega_{DE} = 8\pi\rho_{DE}/(3m_{Pl}^2H_0^2)$  is the density parameter (with  $m_{Pl}$  being the Planck mass and  $H_0$  the Hubble constant). A particular class of quintessence models is characterized by “*tracking*” potentials, for which the field dynamics has a late time accelerating attractor solution, preceded by a period during which the scalar field energy density tracks that of the dominant background component (see Steinhardt, Wang & Zlatev 1999; Zlatev, Wang & Steinhardt 1999). In such models any dependency on the initial conditions is therefore erased, thus alleviating the coincidence problem. Along these lines a full solution to such coincidence is provided by non-minimally coupled scalar field models, where the matter components are directly coupled to the scalar field (see e.g. Amendola 2000; Khoury & Weltman 2004; Alimi & Füzfa 2008)

Precision cosmology offers a unique opportunity to test the nature of dark energy. However, the parameter inference is usually limited by degeneracies amongst the various cosmological parameters, and the combination of several probes is indeed necessary. The imprint of quintessence on the CMB anisotropy power spectrum and the matter power spectrum has been studied in several works (e.g. Viana & Liddle 1998; Caldwell et al. 1998; Perrotta & Baccigalupi 1999; Brax, Martin & Riazuelo 2000). In particular it was shown that a dynamical dark energy component leaves a distinct signature on the CMB through the Integrated Sachs-Wolfe (ISW) effect (Corasaniti et al. 2003), such that models fitting the CMB data, can allow for very different values of the normalization  $\sigma_8$  of the linear matter power spectrum (Kunz et al. 2004). The viability of these models has been tested against CMB and SN Ia data in various works (Corasaniti & Copeland 2002; Baccigalupi et al. 2002; Colombo & Gervasi, 2006). These models can provide fit to the data at the same statistical level of the  $\Lambda$ CDM scenario, implying that cosmological data at redshift higher than  $z \approx 1$  are therefore necessary to further break parameter degeneracies and possibly distinguish between competing DE models.

In recent years there has been a growing interest on whether the clustering of large-scale structures might be crucial for settling the debate on the physical nature of DE. As this process covers a long-period between the dark ages and today ( $0 < z < 1000$ ), it appears as a unique experimentation field for building new tests of DE. Several studies have performed N-body simulations to evaluate the imprint of DE on the non-linear regime of gravitational collapse and determined the signature on the mass power spectrum and cluster mass function (see e.g. Ma et al. 1999; Bode et al. 2001; Lokas, Bode & Hoffman 2004; Munshi, Porciani & Wang 2004). These works have focus on DE models

specified by a constant equation of state, while Benabed & Bernardeau (2001) have performed an analytical study of the growth of matter perturbations for quintessence models at linear and second order respectively, and estimated the effect on the non-linear power spectrum. N-body simulations dedicated to quintessence cosmologies have been performed in various works (Klypin et. 2003; Dolag et al. 2004; Solevi et al. 2006), other studies have also included the gas through N-body hydrodynamical simulations (Maio et al. 2006; Aghanim, da Silva & Nunes 2008). These studies have concluded that the imprint of dark energy on the non-linear matter power spectrum and the cluster mass function at  $z = 0$  remains indistinguishable from the  $\Lambda$ CDM, while significant differences may arise at higher redshifts, with different halo profiles at all redshifts.

A feature common to all these works is the fact that these analysis have exclusively focused on models specified by the same cosmological parameters values, independently of whether these values provide compatible fits of the underlying dark energy model to existing data<sup>1</sup>. This is a crucial point, since it does not allow us to address an important question, namely whether detailed measurements of the non-linear clustering of matter are sensitive to the imprint quintessence/dark energy models which are currently not distinguishable from the standard  $\Lambda$ CDM using SN Ia, CMB and linear matter power spectrum data. This is particularly relevant given the upcoming observational campaigns which will probe with high precision several aspects of the matter clustering. This question will be addressed in this paper, the first of a series dedicated to the imprint of “realistic” dark energy models on the non-linear structure formation. In the upcoming papers we will mostly focus on the physical properties of DM halos: mass functions, density profiles, virialisation process and internal velocity distribution. We will also investigate the spatial halo distribution and the influence on cosmological bias.

The paper is organized as follows: in Section 2 we recall the basic equations describing the dynamics of quintessential cosmologies at the background and linear perturbation level; in Section 3 we present the results of a combined likelihood analysis of the WMAP5-years data and SN Ia from the UNION dataset to constrain two different types of quintessence models specified by Ratra-Peebles and SUGRA potentials respectively. We then identify *realistic* quintessence models which are statistically indistinguishable from the vanilla  $\Lambda$ CDM and discuss their main phenomenological features in Section 4. We use these realistic models as benchmark for studying the structure formation through state-of-the-art N-body simulations which we present in Section 5. We will describe the numerical software developed for the realization of the project, the characteristics of the simulations and discuss the results. In particular we find that quintessence leaves several imprints in the non-linear matter power spectrum at all redshifts and on the non-linear growth of cosmic structures. Finally we will present our conclusion and discuss future work in Section 6.

## 2 QUINTESSENTIAL COSMOLOGY

### 2.1 Basic Homogeneous Equations

Assuming the cosmological principle, the large scale Universe can be considered homogeneous and isotropic and can thus be described by the Friedmann-Lemaître-Robertson-Walker (FLRW) metric, which in terms of the conformal time  $\eta$  reads as:

$$ds^2 = a^2(\eta) \left[ -d\eta^2 + dl^2 \right], \quad (1)$$

where  $a(\eta)$  is the scale factor and  $dl$  is the length element. In this paper, we restrict to spatially flat geometries. Throughout the paper we will use Planck units ( $\hbar = c = 1$ ,  $m_{pl} = 1/\sqrt{G} = 1.2211 \times 10^{19} GeV$ ). We assume the cosmic matter content to consist of pressureless matter (composed of ordinary baryonic matter and cold dark matter), relativistic matter (photons and neutrinos) and a quintessence scalar field. The expansion rate of the Universe, defined in terms of the scale factor by the *Hubble parameter*  $\mathcal{H} = a'/a$  (a prime denotes a derivative with respect to the conformal time  $\eta$ ), is given by the Friedmann equation:

$$\mathcal{H}^2 = H_0^2 \left[ \frac{\Omega_m}{a} + \frac{\Omega_r}{a^2} \right] + \frac{8\pi}{3m_{pl}^2} \rho_Q a^2, \quad (2)$$

with  $H_0$  the Hubble constant and  $\Omega_i = \rho_i/\rho_c$  is the present value of the density parameters, where  $\rho_c = 3H_0^2 m_{pl}^2 / (8\pi)$  is the critical density and  $\rho_i = \rho_m, \rho_r$  indicates respectively the density contribution of pressureless matter and radiation;  $\rho_Q$  stands for the energy density of quintessence.

The quintessence field is assumed to be a neutral (real) scalar field  $\varphi(\eta)$  with self-interaction potential  $V(\varphi)$ , which couples to ordinary matter only through its gravitational influence, (i.e. minimally coupled scalar field). The field dynamics is given by the *Klein-Gordon* equation:

$$\varphi'' + 2\mathcal{H}\varphi' + \frac{a^2}{m_{pl}^2} \frac{dV(\varphi)}{d\varphi} = 0, \quad (3)$$

<sup>1</sup> A noticeable exception is the work of Casarini et al. 2009 in which one of the models considered is compatible with recent data, as derived in La Vacca et al. 2009. However, their approach is rather different than ours and we will discuss some of their results in section 5.5.

where  $\varphi$  is the field expressed in units of the Planck mass. The quintessence energy density and pressure reads as:

$$\begin{aligned}\rho_Q &= \frac{m_{Pl}^2}{2a^2} \dot{\varphi}^2 + V(\varphi), \\ p_Q &= w_Q \rho_Q = \frac{m_{Pl}^2}{2a^2} \dot{\varphi}^2 - V(\varphi).\end{aligned}$$

where  $w_Q$  is the quintessence equation of state.

The evolution of the system is completely determined by specifying the form of the quintessence potential and the scalar field initial conditions ( $\varphi_i, \dot{\varphi}_i$ ), which can be set in the early Universe, for example at the end of inflation. Convenient choices of  $V(\varphi)$  are the so-called *tracking potentials* (see Steinhardt, Wang & Zlatev 1999 and references therein) characterized by a late time scalar field dominated regime, which can be reached from a large range of initial conditions, spreading over dozens of order of magnitudes in the field phase space.

We consider two well-known examples of such potentials. The *Ratra-Peebles* (RP) inverse power law (Wetterich 1988; Ratra & Peebles 1988),

$$V_{RP}(\varphi) = \frac{\lambda^{4+\alpha}}{m_{Pl}^\alpha \varphi^\alpha}, \quad (4)$$

where  $\alpha \geq 0$  and  $\lambda > 0$  are free parameters characterizing the slope and amplitude of the scalar self-interaction. Here we fix the energy scale  $\lambda$  such that for a given value of  $\alpha$  the input value of  $\Omega_Q$  is retrieved. This model was originally proposed to mimic a time-varying cosmological constant (Wetterich 1988), which for nearly flat slopes is recovered at late times, when the scalar field remains frozen at large values by the cosmic expansion. A quintessence inverse power law potential has also been motivated in the framework of supersymmetric extensions of QCD (Binetruy 1999; Masiero, Pietroni and Rosati 2000). However, as noticed by Brax & Martin (2000) for present field values supergravity corrections should be included leading to the following form:

$$V_{SUGRA}(\varphi) = \frac{\lambda^{4+\alpha}}{m_{Pl}^\alpha \varphi^\alpha} e^{4\pi\varphi^2}, \quad (5)$$

which we will refer to as the *SUGRA* model.

## 2.2 Perturbed Quintessential Cosmology

At the inhomogeneous level, assuming small perturbations about the FLRW metric, the linearly perturbed line element in the Newtonian gauge is given by

$$ds^2 = a^2(\eta) \left[ -(1 + 2\Phi(\vec{x}, \eta)) d\eta^2 + (1 - 2\Psi(\vec{x}, \eta)) d\ell^2 \right]. \quad (6)$$

where  $\Phi$  and  $\Psi$  are the Bardeen potentials. Differently from the cosmological constant a quintessential dark energy can cluster and its density perturbations can contribute to the evolution of the gravitational potentials in addition to the perturbations in the other matter components. In order to correctly compute the CMB and the linear matter power spectra, we have modified the CAMB code (Lewis, Challinor & Lasenby 1999) to account both for the modification of the background expansion and the clustering of quintessence. Two equivalent approaches have been adopted to cross-check the validity of the computation. The first is to evolve the perturbations  $\delta\varphi$  of the quintessence field itself through the perturbed Klein-Gordon equation. In the Fourier space we have:

$$\delta\varphi'' + 2\mathcal{H}\delta\varphi' + \left( k^2 + \frac{a^2}{m_{Pl}^2} \frac{d^2V}{d\varphi^2} \right) \delta\varphi + 2\Phi \frac{a^2}{m_{Pl}^2} \frac{dV}{d\varphi} - (3\Psi' + \Phi')\varphi' = 0. \quad (7)$$

The perturbed Einstein equations give the evolution of gravitational potentials  $\Psi$  and  $\Phi$ ,

$$k^2\Psi + 3\mathcal{H}(\Psi' + \mathcal{H}\Phi) = -\frac{4\pi}{m_{Pl}^2} a^2 \rho_s \delta_s, \quad (8)$$

$$\Psi' + \mathcal{H}\Phi = -\frac{4\pi}{m_{Pl}^2} a^2 \rho_s (1 + w_s) v_s, \quad (9)$$

where  $\delta_s, v_s$  and  $w_s$  are the relative density contrast  $\delta\rho_s/\rho_s$ , velocity and equation of state for a given fluid  $s$  (see Eq. (10) for the definition of the quintessence density contrast and velocity in terms of the scalar field perturbation). An implicit summation over all the species  $s$  (photons, baryons, cold dark matter, neutrinos and quintessence) has been assumed. Written in terms of the scalar field perturbation the quintessence density contrast and velocity reads as:

$$\begin{aligned}\frac{a^2}{m_{Pl}^2} \rho_Q \delta_Q &= \varphi' \delta\varphi' + \frac{a^2}{m_{Pl}^2} \frac{dV(\varphi)}{d\varphi} \delta\varphi - \varphi'^2 \Phi \\ v_Q &= -\frac{\delta\varphi}{\varphi'}.\end{aligned} \quad (10)$$

The second approach consists in considering quintessence as an additional fluid, in such a case the quintessence perturbations are characterized by an adiabatic sound speed  $c_A^2 \equiv \frac{p'_Q}{\rho'_Q}$  and an intrinsic entropy perturbation  $\Gamma_Q \equiv \frac{\delta p_Q}{\rho_Q} - \frac{c_A^2}{w_Q} \delta_Q$ . In the framework of quintessence models these quantities take the following form

$$c_A^2 = 1 + \frac{2}{3m_{pl}^2} \frac{dV}{d\varphi} \frac{a^2}{\varphi' \mathcal{H}}, \quad (11)$$

$$\Gamma_Q = \frac{1 - c_A^2}{w_Q} [\delta_Q - 3\mathcal{H}(1 + w_Q)v_Q]. \quad (12)$$

Thus, the continuity and the Euler equation simplify to

$$\begin{aligned} \delta'_Q &= -3\mathcal{H}(1 - w_Q)\delta_Q + (1 + w_Q) \left[ (9\mathcal{H}(1 - c_A^2) + k^2)v_Q + 3\Psi' \right] \\ v'_Q &= -\frac{\delta_Q}{1 + w_Q} + 2\mathcal{H}v_Q - \Phi. \end{aligned} \quad (13)$$

For super-Hubble scales,  $k\mathcal{H}^{-1} \ll 1$ , the tracking properties of the self-interaction potential force the quintessence perturbations to follow a tracking solution as well (see Brax, Martin & Riazuelo 2000). A departure from this regime occurs when the mass term  $k^2$  in Eq. (7) becomes non-negligible. Therefore, we assume that for all observable modes, the quintessence perturbations reach the tracking solution before becoming non-negligible; this simplifies the choice of initial conditions. In fact it allows us to assume quintessence to be initially homogeneous.

### 3 SUPERNOVA AND CMB LIKELIHOOD ANALYSIS

In this section, we present the results of the combined likelihood analysis of the latest SN Ia and CMB data. Our goal is to identify quintessence models characterized by a set of parameters  $(\alpha, \Omega_m)$ , which are statistically consistent with the observations (within  $2\sigma$ ), while departing from the standard  $\Lambda$ CDM values. These sets of parameters define what we call realistic quintessence models.

SNe Ia standard candles provide a measurement of the luminosity distance  $d_L(z)$ ,

$$d_L(z) = (1 + z)H_0^{-1} \int_0^z \frac{dz'}{E(z')}, \quad (14)$$

with  $E(z) = H(z)/H_0$  is the dimensionless Hubble parameter and  $z = 1/a - 1$  is the cosmological redshift. Hence, the Hubble diagram leaves  $H_0$  unconstrained and degenerate in the plane  $\alpha - \Omega_m$  (Caresia, Matarrese & Moscardini 2004; Schimd et al. 2007). Therefore, we infer constraints from SN data after marginalizing analytically the  $\chi^2$  over  $H_0$  (Lewis & Bridle 2002; Di Pietro & Claeskens 2004). The CMB angular power spectrum is also degenerate in  $\alpha - \Omega_m$  and  $H_0 - \alpha$  planes, however these degeneracies are nearly orthogonal to those in the luminosity distance, thus providing improved parameter bounds. In addition under the flat geometry prior, CMB data allow for a precise measurement of  $\Omega_m h^2$  and  $\Omega_b h^2$  (where  $h = H_0/100$  km/s Mpc $^{-1}$ ), as well as the primordial power spectrum properties (amplitude and slope).

We perform a combined analysis of the WMAP5-yrs CMB power spectra (Komatsu et al. 2008) and the recent compilation of SN Ia measurements, UNION dataset (Kowalski et al. 2008). We run a series of Markov Chains Monte Carlo using the publicly available codes CAMB and CosmoMC (Lewis, Challinor & Lasenby 1999; Lewis & Bridle 2002), properly modified to correctly account for the physics described in the previous section (influence of quintessence and its perturbations). We assume uniform priors on the following parameters:  $\Omega_b h^2$ ,  $\Omega_{DM} h^2$ ,  $h$ ,  $\alpha$ ,  $n_S$ ,  $A_S$ ,  $z_{rec}$ , and marginalize over  $A_{SZ}$  (see Komatsu et al. 2008 for the exact definitions).

The results of the combined analysis are summarized in figure 1, where we plot the 1 and  $2\sigma$  confidence regions in the plane  $\Omega_m h^2 - \alpha$  for the RP (top panel) and SUGRA (bottom panel) models respectively. As it can be seen the concordance  $\Lambda$ CDM model, which corresponds to the limiting value  $\alpha \rightarrow 0$  of the quintessence parameter, is within the  $1\sigma$  confidence region. As noticed in previous quintessence/dark energy data analysis (see for instance Corasaniti et al. 2004) quintessence models tend to fit the data by requiring lower values of  $\Omega_m h^2$ , also confirmed by the orientation of the degeneracy line in the  $\Omega_m h^2 - \alpha$  plane. As we will discuss more in detail in the next Section, this is because models with  $\alpha > 0$  are characterized by a less accelerated cosmic expansion, therefore under the flatness requirement, they require a larger amount of dark energy (lower matter density) to account for the data. In Table 1 we show the marginalized confidence intervals on the model parameters for RP and SUGRA respectively.<sup>2</sup>

In figure 1 we mark the model parameter values assumed in previous works dedicated to the study of the effect of quintessence on

<sup>2</sup> It is worth noticing that supernova data do not provide strong constraints on slope and amplitude of the SUGRA potential. This is expected since the exponential term in Eq. 5 is dominant at late times, leaving these parameters almost completely degenerate as shown by Caresia, Matarrese & Moscardini (2004), and retrieved in Schimd et al. (2007).

Parameters	RPCDM	SUCDM
$\Omega_b h^2$	$0.0226 \pm 0.0012$	$0.0227 \pm 0.0013$
$\Omega_{DM} h^2$	$0.107^{+0.012}_{-0.011}$	$0.105^{+0.012}_{-0.013}$
$h$	$0.674^{+0.047}_{-0.048}$	$0.661^{+0.055}_{-0.058}$
$z_{reion}$	$10.4 \pm 2.7$	$10.6 \pm 2.8$
$10^9 A_S$	$2.12^{+0.18}_{-0.17}$	$2.11^{+0.19}_{-0.17}$
$n_s$	$0.964^{+0.028}_{-0.029}$	$0.968^{+0.034}_{-0.030}$
$\alpha$	$< 0.89$	$< 6.2$
Derived parameters		
$\Omega_m h^2$	$0.130 \pm 0.012$	$0.128 \pm 0.013$
$\Omega_m$	$0.287^{+0.056}_{-0.050}$	$0.293^{+0.060}_{-0.053}$
$\sigma_8^{lin}$	$0.737^{+0.083}_{-0.097}$	$0.70^{+0.11}_{-0.15}$
$\log_{10} \lambda (GeV)$	$-8.9^{+3.3}_{-2.0}$	$-3.7^{+12.5}_{-6.8}$
$w_0$	$< -0.78$	$< -0.83$
$w_1$	$< 0.11$	$< 0.39$
$q_0$	$0.44^{+0.13}_{-0.17}$	$0.47^{+0.13}_{-0.16}$
$z_{acc}$	$0.67^{+0.15}_{-0.16}$	$0.58^{+0.18}_{-0.19}$
$z_d$	$0.42^{+0.12}_{-0.11}$	$0.40^{+0.12}_{-0.11}$
$t_0 (Gyr)$	$13.84^{+0.28}_{-0.27}$	$13.95^{+0.38}_{-0.32}$

**Table 1.** Cosmological parameters and their 95% confidence level intervals obtained from the combined analysis of WMAP5 and UNION SN Ia data.  $w_0$  is the present value of the DE eos and  $w_1$  is the first order parameter of the linear eos parameterization  $w(a) = w_0 + w_1(a - 1)$  (Chevallier & Polarski, 2001 ; Linder, 2003, quintessence only allows  $w_0 > -1$  and  $w_1 > 0$ ),  $q_0$  is the present value of the acceleration factor,  $z_{acc}$  is the redshift marking the beginning of cosmic acceleration,  $z_d$  is the redshift of DE domination),  $A_S$  is the primordial amplitude of curvature perturbations at  $k = 0.05 \text{Mpc}^{-1}$ .

structure formation (Klypin et al. 2003 ; Dolag et al. 2004 ; Solevi et al. 2006). These works have all assumed  $\Omega_m = 0.3$  and  $h = 0.7$ , corresponding to optimal fit parameter values of  $\Lambda$ CDM cosmologies. Dolag et al. (2004) considered the case  $\alpha = 0.6$  for RP and  $\alpha = 6.7$  for SUGRA (open circle), both leading today ( $z = 0$ ) to an equation of state parameter  $w_Q = -0.83$ . Klypin et al. (2003) (see also Solevi et al. 2006) have assumed the amplitude of the scalar potential to be  $\lambda = 1 \text{ TeV}$ , which for  $\Omega_m = 0.3$  corresponds to  $\alpha \approx 4$  for both Ratra-Peebles and SUGRA models (star) and gives a present eos  $w_Q = -0.5$  and  $w_Q = -0.85$ , respectively. Maio et al. (2006) have also considered a SUGRA potential and assumed  $\alpha = 6.5$  (cross). It is evident that such models are ruled out at more than  $2\sigma$  by current CMB and SN Ia data. In addition these works have assumed the same value of the total matter density as inferred in a  $\Lambda$ CDM cosmology, hence it is not surprising that the authors have concluded that in quintessence models the present structure formation process, especially on the non-linear scales, slightly depart from the  $\Lambda$ CDM scenario. An exception to the approach of these works is the recent analysis by Casarini et al. (2009) which considered a Sugra model with  $\Omega_m = 0.255$  and  $\alpha_Q = 2.2$  (• in Figure 1) corresponding to an eos value today  $w_0 = -0.908$  ( $h = 0.7$ ), parameters inferred in another study by La Vacca et al. (2009).

In contrast we aim to study realistic models of quintessence which differ from the  $\Lambda$ CDM, while being statistically consistent with current cosmological data at level of significance that does not allow them to be distinguished from the  $\Lambda$ CDM. We choose a  $\Lambda$ CDM, RP and SUGRA model specified by the parameter values given in Table 2. These are within the  $2\sigma$  confidence limits, thus differences of their  $\chi^2$  values are not statistically significant. The RP and SUGRA realistic model parameters are plotted in figure 1 as cross marks. We want to stress that the inferred constraints on  $n_s$ , as well as its best fit values are nearly similar for the three different cosmologies (see Table 1), therefore without loss of generality we assume  $n_s = 0.963$ . For the Hubble parameter we assume  $h = 0.72$ , corresponding to the best fit value for a  $\Lambda$ CDM cosmology (Komatsu et al. 2008). Although the marginalized values of  $h$  for RP and SUGRA models are slightly lower (see Table 1), the value assumed is within the 95% confidence interval. Such a choice allows us to directly compare physical scales between different N-body simulations. Hereafter  $\Lambda$ CDM will denote the concordance model, RPCDM quintessence with Ratra-Peebles potential Eq. (4) and SUCDM quintessence with SUGRA potential Eq. (5).

#### 4 PHENOMENOLOGY OF REALISTIC QUINTESSENCE MODELS

Here we describe the main features of the realistic quintessence cosmologies which we inferred from the likelihood data analysis described in the previous section and for which we aim to study the non-linear structure formation through N-body simulations. Although the characteristics of the background evolution and the linear density perturbations for the RP and SUGRA models, and more in general time varying

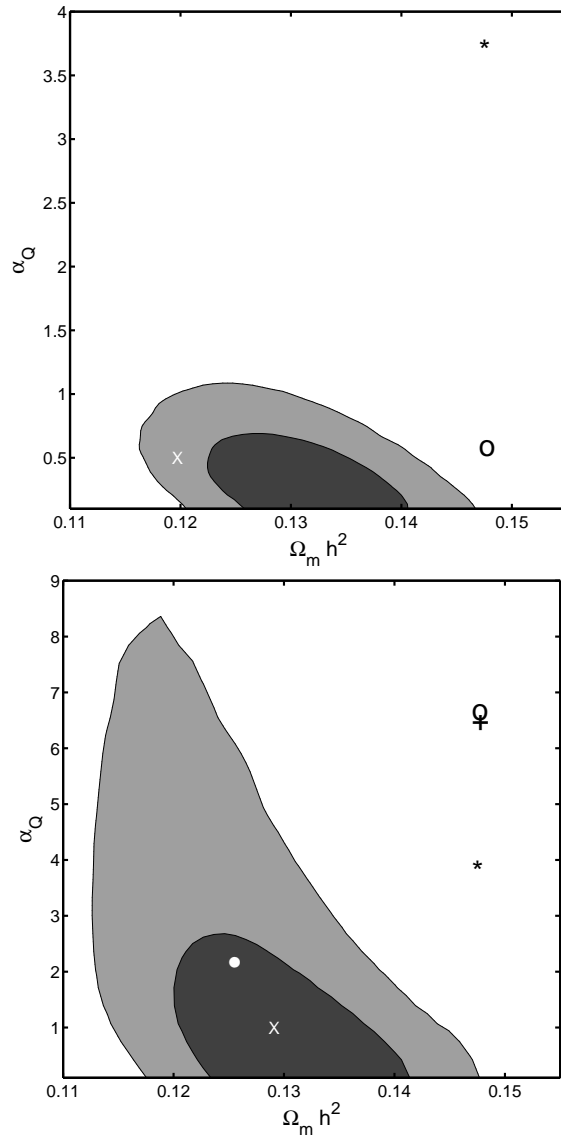


**Figure 1.** 68% and 95% confidence regions in the  $\Omega_m h^2 - \alpha$  plane from the combined analysis of the UNION SN Ia Hubble diagram and WMAP-5yrs CMB data for the Ratra-Peebles (top panel) and SUGRA (bottom panel). A cross mark (X) indicates our realistic quintessence model parameters choice, while model parameter values assumed in the literature are marked with \* (Klypin et al. 2003 and Solevi et al. 2006), o (Dolag et al. 2004), + (Maio et al. 2006), • (Casarini et al. 2009).

Parameters	$\Lambda$ CDM	RPCDM	SUCDM
$\Omega_m$	0.26	0.23	0.25
$\alpha$	0	0.5	1
$A_S$	$2.1 \times 10^{-9}$	$2.0 \times 10^{-9}$	$2.1 \times 10^{-9}$
Derived parameters			
$\sigma_8^{lin}$	0.80	0.66	0.73
$\lambda(\text{eV})$	$2.4 \times 10^{-3}$	4.9	$2.1 \times 10^3$
$w_0$	-1	-0.87	-0.94
$w_1$	0	0.08	0.19

**Table 2.** Cosmological parameters selected for the realistic models. These are flat models ( $\Omega_{Q(\Lambda)} = 1 - \Omega_m$ ), with a spectral index  $n_s = 0.963$ ,  $h = 0.72$ ,  $\Omega_b h^2 = 0.02273$ , and  $\tau = 0.087$  corresponding to  $z_{reion} = 10.1$  for RPCDM and  $z_{reion} = 10.4$  for SUCDM respectively.

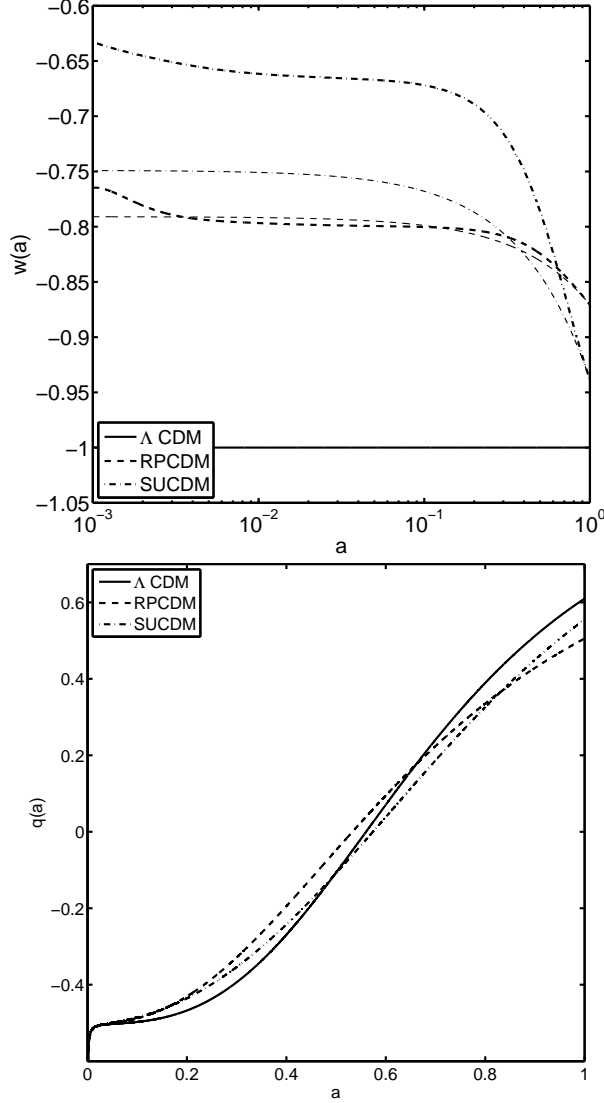


**Figure 2.** Evolution of the equation of state  $w = p/\rho$  (top panel) and acceleration factor  $q = \mathcal{H}'/\mathcal{H}^2$  (bottom panel) as function of the scale factor  $a$  for the models in Table 2. For comparison we also plot the linear eos parametrization for each model.

dark energy equation of state models have been studied in a vast literature, we think that the reader may benefit from a brief review of how the scalar field dynamics impact the cosmic expansion and the evolution of the matter perturbations. In fact this will allow for a necessary understanding of the effects that dark energy leaves on the non-linear structure formation which will be discussed in the next section.

Quintessence affects the linear clustering of matter through the combined effect on the background evolution and the presence of dark energy perturbations.

Let us first focus on the background dynamics of quintessence models. In the top panel of figure 2 we plot the evolution of the quintessence eos as a function of the scale factor for the RPCDM (dash line) and SUCDM (dash-dot line) models, and the  $\Lambda$ CDM (solid line) respectively. We can see that these curves are characterized by different behaviors which are indicative of the different cosmic expansion histories. In particular we may notice that during the matter dominated era the quintessence eos is nearly constant (consistently with the fact that the field is in the tracker solution), with the SUCDM eos larger than the RPCDM case, while at later times it rapidly evolves with the SUGRA eos becoming more negative than in the RP case. This is because at early times the field is evolving over an inverse power law potential and since the RP model considered is flatter than SUGRA (i.e. the slope  $\alpha_{RP} < \alpha_{SUGRA}$ ), hence  $w_{RP} < w_{SUGRA}$  during the matter dominated era, and the flatter the potential the smaller is the variation of the equation of state. In contrast at late times (when  $\varphi \approx 1$ ) in the SUGRA model the field rolls over a region where the contribution of the exponential term in Eq. (5) is important, thus making the curvature smaller than that of RP, thus the kinetic energy rapidly decreases causing the present SUGRA eos value to be more negative than



the RP case. In figure 2 (top panel) we also plot the linear eos parameterization,  $w(a) = w_0 + w_1(1 - a)$  (Chevallier & Polarski 2001; Linder 2003), which are commonly used in the literature to mimic the quintessence model dynamics. We may notice that such parameterization provide a valid approximation at low redshift, on the other hand during the matter dominated era it can account for the quintessence evolution only reasonably well for very flat potentials. More specifically, the accuracy of this parameterization at  $z \approx 1000$  varies from about 4% for the RPCDM to 15% for the SUCDM. This specific behaviours of the quintessence equation of state affects the cosmic expansion history, as it can be seen in the bottom panel of figure 2 where we plot the acceleration factor  $q = \mathcal{H}'/\mathcal{H}^2$  for the three different realistic models. Deep in the radiation dominated  $q = -1$  for all models, while the subsequent evolution during the matter-dominated era differs. We can see that before the deceleration-to-acceleration transition takes place (corresponding to  $q$  changing sign),  $|q_{\Lambda\text{CDM}}| > |q_{\text{QCDM}}|$ , thus indicating that the  $\Lambda\text{CDM}$  model decelerates more than in realistic quintessence cosmologies. The acceleration occurs nearly at the same redshift for all models, although for the specific model parameter choice we have that RPCDM accelerates slightly earlier than the  $\Lambda\text{CDM}$  and SUCDM. On the other hand for  $a > 0.6$  we have  $q_{\Lambda\text{CDM}} > q_{\text{QCDM}}$ , hence the acceleration in  $\Lambda\text{CDM}$  is stronger than in quintessence models, which implies that in order to fit the data as well as the  $\Lambda\text{CDM}$ , the smaller acceleration of the quintessence cosmologies is compensated by a larger amount of dark energy density, i.e. (in a flat universe) a smaller amount of matter. This is indeed the case, since for our realistic models for which we have  $\Omega_m = 0.23$  for the RPCDM and  $\Omega_m = 0.25$  for the SUCDM while  $\Omega_m = 0.26$  in  $\Lambda\text{CDM}$  (see Table 2). The different cosmic expansion histories affect the linear evolution of the matter density perturbations in a rather peculiar way resulting in a suppression of their growth rate at late times. This can be understood by consider the equation for the linear growth factor of the matter density perturbations,  $D_+(a)$ :

$$\frac{d^2 D_+}{da^2} + \left( \frac{d \ln \mathcal{H}}{da} + \frac{2}{a} \right) \frac{dD_+}{da} - \frac{3\Omega_m H_0^2}{2a^3 \mathcal{H}^2} D_+ = \frac{1}{a^2 \mathcal{H}^2 T_m(k)} \left( \frac{\alpha^2 \delta\varphi}{m_{pl}^2} \frac{dV}{d\varphi} - 2a^2 \mathcal{H}^2 \frac{d\varphi}{da} \frac{d\delta\varphi}{da} \right) \quad (15)$$

where  $T_m(k)$  is the matter transfer function. Since we aim to isolate the effect of the background evolution from that of the dark energy perturbations let us neglect for the moment the feedback of the quintessence field fluctuations, and set to zero the right-hand-side of Eq. (15). We may notice that in such a case the evolution of the growth factor becomes scale-independent. In figure 3 (top) we plot the normalisation of the linear matter power spectrum (through the *rms* mass fluctuation amplitude  $\sigma_8(a)$  in spheres of size  $8h^{-1}$  Mpc) for the three realistic models. As already mentioned the growth factor in quintessence cosmologies is suppressed at late times compared to the  $\Lambda\text{CDM}$  case. As can be seen in figure 3 (bottom), on such a scale the presence of quintessence perturbations increases the power suppression by a few percent at  $z = 0$  (see also figures 5 and 6 for the spatial dependence of this effect).

In fact quintessence perturbations cause an additional scale dependent effect on the linear clustering of matter. A simple way to evaluate such a scale dependence is to consider quintessence as a fluid with comoving Jeans-mode given by the curvature of the potential, i.e. the mass of the field,  $k_J = a/m_{pl} \sqrt{d^2 V/d\varphi^2}$ . Therefore, scales which correspond to modes  $k < k_J$  will collapse under gravitational instability, while modes  $k > k_J$  will undergo a series of damped oscillations due to pressure waves in the quintessence fluid. Since quintessence is a light field, by the time it becomes the dominant energy component its clustering has halted on the small scales, while allowing for some level of clustering on the larger ones. In figure 4 we plot the redshift evolution of  $k_J$  for the RPCDM and SUCDM models respectively. We can see that at  $z = 0$  the Jeans-scale correspond to  $k_J \approx 3 \times 10^{-4} \text{Mpc}^{-1}$ , hence today only quintessence perturbations which are on the very large scales can cluster.

This has two major consequences. Firstly, the large scale clustering of dark energy enhances the amplitude of the ISW effect on the CMB power spectrum (Corasaniti et al. 2003; Lewis and Weller 2003), as it can be seen in figure 5 where we plot the ratio of the CMB temperature power spectrum of the realistic models with and without quintessence perturbations. Secondly, on the small scales where dark energy is nearly homogeneous, the growth factor is suppressed due to the effect of the background dynamics. Therefore in combination with the power enhancement on the large scales caused by the dark energy perturbations, the overall effect of quintessence on the linear matter power spectrum is to produce a different distribution of power between the small and large scales with respect to the  $\Lambda\text{CDM}$  scenario.

This can be seen in figure 6 where we plot the CMB normalized linear matter power spectra (top panel), and the ratio of the linear matter power spectra with and without quintessence perturbations (bottom panel) for the realistic models. From the latter we can clearly see that on the very large scales ( $k < k_J$ ) the dark energy clustering enhances the matter power spectrum compared to the unclustered case, while on small scales ( $k > k_J$ ) the opposite occurs. This is consistent with the results of Ma et al. (1999), where the authors showed that for increasing values of a constant eos the amount of dark matter clustering on the large scales is enhanced, while on small scales it remains unchanged when compared to the  $\Lambda\text{CDM}$  case. Consequently when considering CMB normalized spectra, quintessence models generally predict smaller values of the  $\sigma_8$  than the  $\Lambda\text{CDM}$  as shown by Kunz et al. (2004)

Indeed not including the effect of the dark energy perturbations would lead to overestimated values of  $\sigma_8$ ; for instance assuming a homogeneous quintessence we find  $\sigma_8 = 0.68$  for the RPCDM model (instead of 0.66) and  $\sigma_8 = 0.76$  (instead of 0.73), corresponding to a loss of about 3% and 4% for RP and SUGRA respectively (see also bottom panel of figure 3). Accounting for dark energy perturbations requires solving Eq.(15) with a non-vanishing rhs, and results in a lowering of the homogeneous solution ( $\delta\varphi = 0$ ) for the linear growing mode  $D_+(a)$ .

We find the WMAP normalized linear matter power spectra, when evaluated including the effect of dark energy clustering, are statistically consistent with the power spectrum estimates from the Sloan Digital Sky Survey data (SDSS, Tegmark et al. 2006). For consistency we

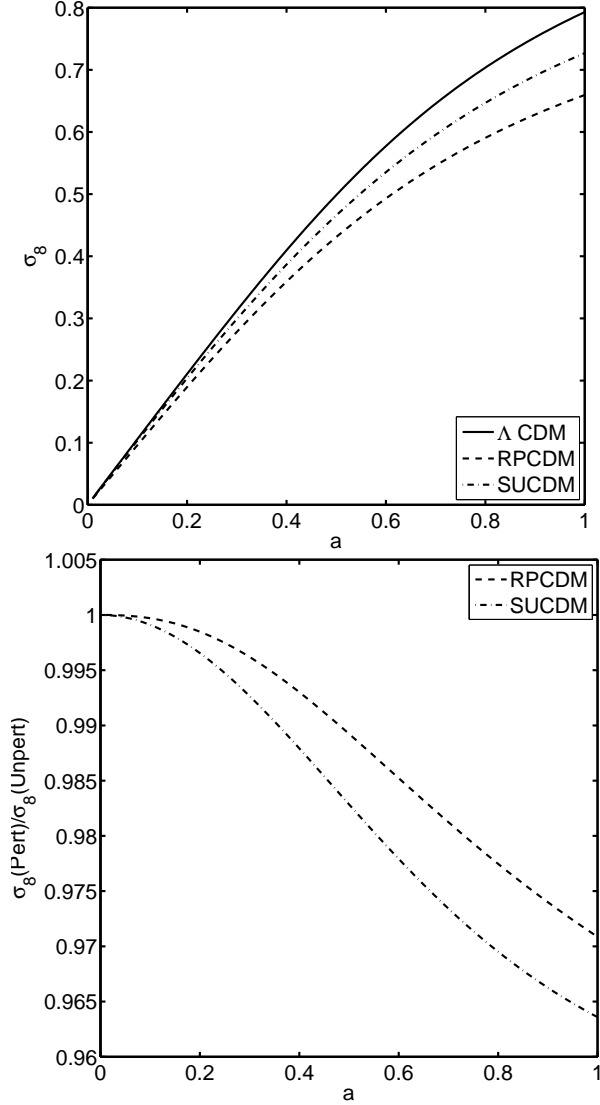


**Figure 3.** Evolution of the  $\sigma_8$  parameter for the models in Table 2 (top). Reshift evolution of the ratio of the  $\sigma_8$  value with and without quintessence perturbations (bottom).

limit to the reduced dataset including point up to  $k = 0.2h^{-1}\text{Mpc}$  which are not affected by non-linear corrections. The three realistic models best fit the SDSS data with  $\chi^2$  differences smaller than unity, provided the galaxy bias parameter,  $b_g$ , assumes the following values:  $b_g = 2.02$  for RPCDM,  $b_g = 2.01$  for SUCDM and  $b_g = 1.98$  for  $\Lambda$ CDM.

It is worth remarking that the effects due to the background evolution and clustering of quintessence are strictly related to the features of the quintessence potential. Although the scalar potential can be expressed in terms of time derivatives of the equation of state parameter (see e.g. Dave et al. 2002), the simplest eos parametrizations used in previous works can at most reproduce the quintessence dynamics only at very small redshift, failing to describe features related to the scalar potential and its higher derivatives at high redshift. Such features can in principle be accounted for only when using more complicated multi-dimensional parametrizations. Therefore, the results of N-body simulations of dark energy models specified by a constant or a linearly scale factor evolving equation of state are intrinsically incomplete with respect to the fundamental scalar field evolution approach that we have developed in this study.

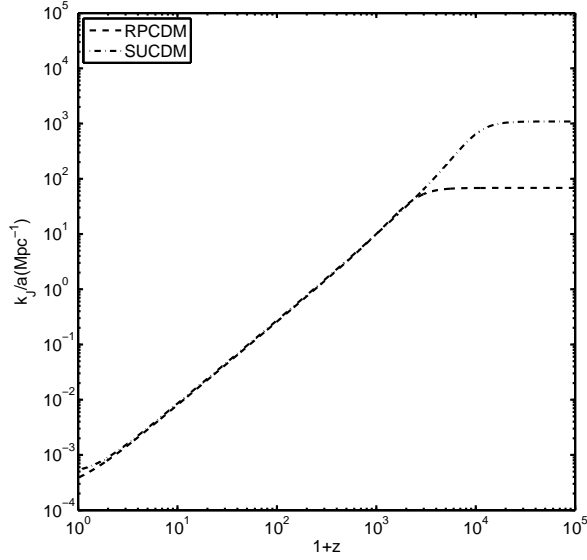


**Figure 4.** Reshift evolution of the physical Jeans wavenumber  $k_J/a = \frac{1}{m_{Pl}} \left( \frac{d^2 V}{d\psi^2} \right)^{1/2}$  associated to the quintessence fluid.

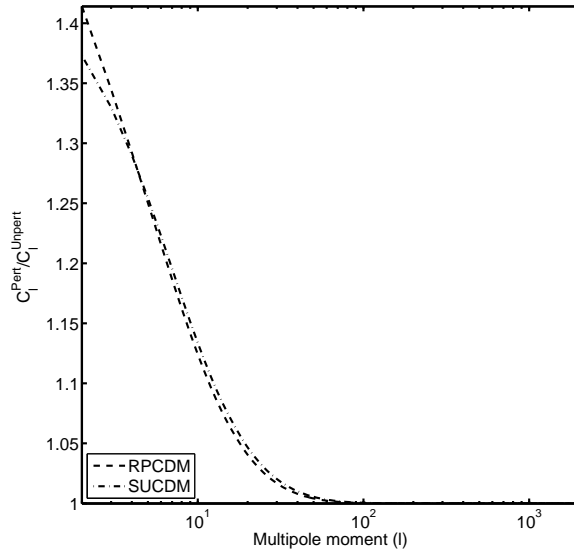


**Figure 5.** Ratio between the angular power spectrum of the CMB anisotropies with and without quintessence perturbations for the models in Table 2.

## 5 THE NON-LINEAR MATTER POWER SPECTRUM

In this section, we present the N-body simulations that we have performed to study the imprints of realistic quintessence cosmologies on the non-linear structure formation. We will first introduce the numerical methods developed, then we will describe the characteristics of the cosmological simulations and finally discuss the results.

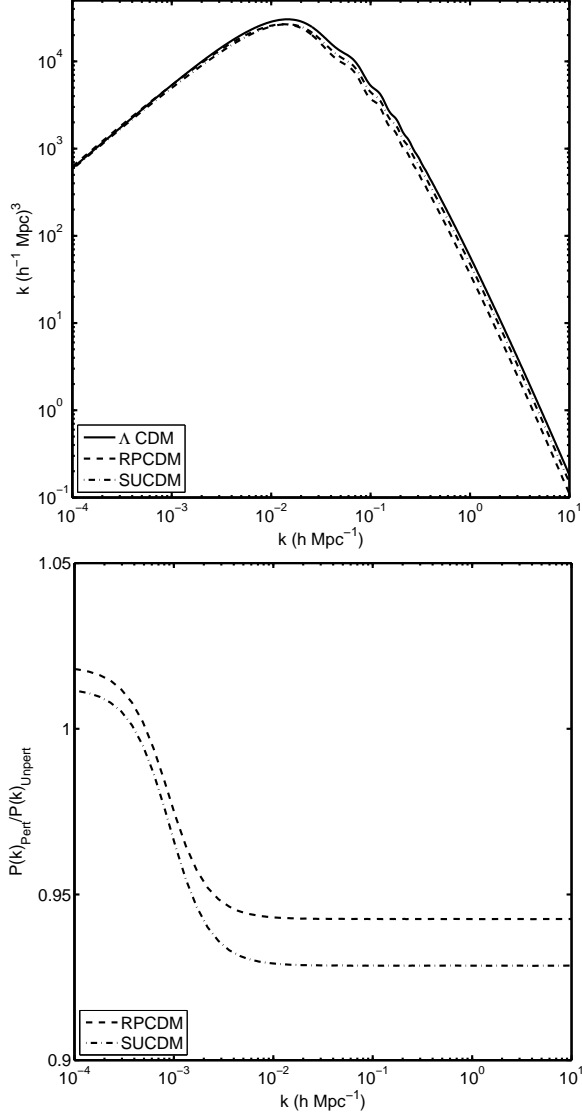


**Figure 6.** CMB-normalized linear matter power spectra for the models in Table 2 (top panel). Ratio between the power spectrum with and without quintessence perturbations (bottom panel).

### 5.1 Initial conditions

The initial conditions for the numerical simulations have been calculated using the MPGRAFIC package described in great details in Prunet et al. (2008). This code is a parallel version of GRAFIC (Bertschinger 1995; Bertschinger 2001) and generates gaussian random fields<sup>3</sup>. Initial displacements and velocities of the dark matter particles are computed using the Zel'dovich approximation at early cosmic time  $\tau$ ,

$$\mathbf{x}(\mathbf{q}, \tau) = \mathbf{q} + \frac{D_+(\tau)}{D_+^0} \mathbf{d}(\mathbf{q}), \quad (16)$$

$$\mathbf{v}(\mathbf{q}, \tau) = \frac{\dot{D}_+(\tau)}{D_+^0} \mathbf{d}(\mathbf{q}), \quad (17)$$

where  $\mathbf{x}$  is the perturbed comoving position,  $\mathbf{v}$  is the proper peculiar velocity,  $\mathbf{q}$  is the Lagrangian coordinate corresponding to the unperturbed comoving position. The dot denotes a derivative with respect to  $\tau$  and  $\mathbf{d}(\mathbf{q})$  is the displacement field computed from the density fluctuation

<sup>3</sup> We however note that MPGRAFIC does not use any Hanning filter unlike the default version of GRAFIC. This is important, especially for large scale simulations, because the Hanning filter damps out small scale modes.

field. The latter is obtained as convolution of a random white noise (which defines the phase of the realization of the Universe) with the square root of the linear power spectrum (which defines the amplitude of the fluctuations at different scales).

The public version of MPGRAFIC includes dark energy only as a cosmological constant, in order to adapt the code to quintessence cosmologies, we have first input MPGRAFIC with the power spectrum at  $z=0$  computed with the modified version of CAMB (described in the previous section). Then, we have modified all the cosmological routines (such as  $a(\tau)$ ,  $D_+(\tau)$  and  $\dot{D}_+(\tau)$ ) to account for the quintessence effects. In particular, the growth factor routine was modified to account for Eq. (15) (with homogeneous quintessence and a vanishing right-hand-side as explained above and in section 5.2). In those quintessential universes, DE dominates lately in expansion history (at  $z_d < 0.45$  see Table 1) so that the initial conditions for  $D_+(a)$  for very small  $a$  correspond to matter dominated Einstein-deSitter cosmology<sup>4</sup>. We have cross-checked the obtained growth factor with the solution computed by the CAMB code in the case of vanishing DE perturbations. At this point, some important remarks are necessary concerning the generation of the initial conditions. For each cosmological simulation we have considered the same realization of the Universe, that is to say we have used the same white noise (more specifically the Horizon white noise<sup>5</sup>). This choice allows us to properly compare the results between different models. As far as the choice of the initial redshift is concerned, we started all simulations with the same amount of fluctuations at the scale of the grid resolution which is given by  $\sigma(L/n, z_i)$ , where  $L$  is the box length and  $n$  is the number of coarse grids along one spatial direction. Again this requirement allows us to consistently compare different models. The initial redshift  $z_i$ , then depends on the cosmology and box length considered, and is determined by solving the equation

$$\frac{\sigma(L/n, z_i)}{\sigma(L/n, z=0)} = \frac{D_+(z_i)}{D_+(z=0)},$$

where  $D_+(z)$  is the linear growing mode obtained solving Eq. (15) without quintessence perturbations ( $\delta\varphi = 0$ ). As we will discuss more clearly in the next section this is because the N-body simulation code does not account for the gravitational collapse of quintessence (see section 5.2 below). On the other hand  $\sigma(L/n, 0)$  is obtained using the linear matter power spectrum at  $z = 0$  calculated including the effect of quintessence perturbations (see sections 4 and 5.2), and  $\sigma(L/n, z_i)$  is fixed to a small arbitrary value. We choose  $\sigma(L/n, z_i) = 0.05$ , for which we expect small artificial effects due to the Zel'dovich approximation to be small. In fact, Crocce et al. (2006) by using an accurate second-order Lagrangian Perturbation Theory (2LPT) to set-up the initial conditions, have shown that a late time start of the N-body simulations using the Zel'dovich approximation tends to underestimate the non-linear power spectrum at the level of 2%–8% (depending on the redshift). In their analysis the initial redshift of the simulations is set to  $z_i = 49$ . In our case, by using the above method and considering the same cosmology and simulation box length we have  $z_i = 72$ , which is high (and even much higher than  $z_i = 30$  used in Smith et al. 2003). Finally it is worth stressing that our analysis mainly focus on the difference between models. Therefore, spurious effects caused by the Zel'dovich approximation are expected to be negligible, and unlikely to affect our main conclusions.

## 5.2 Cosmological code

The N-body simulations have been performed using the RAMSES code (Teyssier 2002; Rasera & Teyssier 2006), which is based on an Adaptive Mesh Refinement (AMR) technique, with a tree-based data structure that allows for recursive grid refinements on a cell-by-cell basis. Particles are evolved using a particle-mesh (PM) solver, while the Poisson equation is solved by a multigrid method. The refinement strategy follows a “quasi-lagrangian” approach where cells are divided by 8 if their enclosed masses are multiplied by 8. We did not impose any maximum level of refinement for the simulations, and let the code trigger as much refinement levels as needed. This allows us to have very high resolution down to the core of dark matter halos (up to  $2.5 \text{ h}^{-1} \text{ kpc}$ ). RAMSES has been parallelized using a dynamical domain decomposition based on the Peano-Hilbert space-filling curve. This is an important improvement of the code for high-resolution runs with a high level of structuration. In order to implement the cosmological evolution of the different models we have modified all cosmological routines such as to render them model-independent. These are now input with pre-computed numerical tables of cosmological quantities needed to fully specify the cosmological model evolution. In order to check that the overall implementation is correct, we compare the evolution of the power spectrum on the large scales ( $> 500 \text{ Mpc}$ ) to the prediction of the linear calculation using the CAMB code and find an agreement at the percent level.

Ideally, the gravitational collapse of quintessence should be incorporated in the N-body code. However, the collapse of a negative pressured quintessence fluid is a very complicated task that will require, in addition, a considerable amount of numerical resources to the detriment of precision on the matter fluctuations. A naive approach would consist of linearly propagating the matter power spectrum starting from some initial conditions set deep in the radiation era till the initial redshift of the simulation. Nonetheless using such an approach would completely miss the late time influence of quintessence perturbations, thus failing to reproduce the correct linear matter power spectrum at  $z = 0$  at least on those large scales that evolve linearly in the simulation box. A better approximation is realized by using the linear

<sup>4</sup> In practice, we chose  $D_+(a_i = 0.002) = 0.6a_i$  and  $(dD_+/da)|_{a_i} = 0.6$  (see also Peebles, 1993). Note that only the quantity  $D_+(a)/D_+(a_0 = 1)$  matters in the normalisation of cosmological initial conditions.

<sup>5</sup> <http://www.projet-horizon.fr>

Parameters	162 h <sup>-1</sup> Mpc	648 h <sup>-1</sup> Mpc	1296 h <sup>-1</sup> Mpc
$z_{\text{in}}$	93	56	41
$m_p(\text{h}^{-1} M_{\odot})$	$2.28 \times 10^9$	$1.46 \times 10^{11}$	$1.17 \times 10^{12}$
$\Delta_x(\text{h}^{-1}\text{kpc})$	2.47	19.78	39.55
$l_{\text{max}}$	7	6	6
$z_{\text{in}}$	81	50	37
$m_p(\text{h}^{-1} M_{\odot})$	$2.02 \times 10^9$	$1.30 \times 10^{11}$	$1.04 \times 10^{12}$
$\Delta_x(\text{h}^{-1}\text{kpc})$	2.47	19.78	39.55
$l_{\text{max}}$	7	6	6
$z_{\text{in}}$	92	55	40
$m_p(\text{h}^{-1} M_{\odot})$	$2.20 \times 10^9$	$1.41 \times 10^{11}$	$1.13 \times 10^{12}$
$\Delta_x(\text{h}^{-1}\text{kpc})$	2.47	19.78	39.55
$l_{\text{max}}$	7	6	6

**Table 3.** Simulation parameters for the  $\Lambda$ CDM, RPCDM and SUCDM cosmologies from top to bottom. Each simulation contains  $512^3$  particles with  $512^3$  coarse-grid cells and has been evolved up to  $z = 0$ . The various entries report the values of the simulation initial redshift  $z_{\text{in}}$ , particle mass  $m_p$ , spatial resolution  $\Delta_x$  and maximal number of refinements  $l_{\text{max}}$ .

matter power spectrum at  $z = 0$  computed from the linear perturbation theory accounting for the presence of quintessence perturbations (for instance using the CAMB code), then evolve backwards such a spectrum to the starting redshift of the simulation by using the linear growing mode  $D_+(a)$  evaluated without including the quintessence perturbations. In such a case, we are guaranteed by construction that the evolution of dark matter particles on the scales that remains linear in the N-body simulation recovers the matter power spectrum at  $z = 0$  when quintessence perturbations are included. An ideal quintessence simulation would account for more subtle effects, such as a coupling between the non-linear evolution of DM on the small scales and the linear clustering of DE on the large ones, as well as a coupling between the non-linear clustering of DM and that of DE on the small scales. Developing such a simulation requires a study that goes beyond the scope of our analysis and we leave it for future work. Nevertheless, we think that our approach by including the effect of the large scale linear evolution of DE perturbations is an important improvement compared to previous N-body simulation studies which have implemented dark energy only through its effects on the background evolution.

### 5.3 Simulations set

The scope of this series of articles is to accurately investigate the imprints of realistic dark energy models on the cosmic structure formation. To this end we perform a set of simulations with different box lengths, which allows us to precisely evaluate the dark energy effects at different scales. For numerical reasons, we need to compromise between a spatial resolution small enough to follow the formation of halos, and a volume box sufficiently large such as to provide sufficient statistics. We have therefore run simulations for three different box sizes, probing scales from kpc to Gpc: the largest box with  $L = 1296 \text{ h}^{-1}\text{Mpc}$  provides us a good statistics on cluster counts; while the smallest box with  $L = 162 \text{ h}^{-1}\text{Mpc}$  has sufficient spatial resolution for accurate measurements of the halo density profiles. An intermediate box with  $L = 648 \text{ h}^{-1}\text{Mpc}$  is a good compromise for probing both the linear and non-linear scales of the matter power spectrum which we discuss in this paper. Because of the spatial and mass resolution we expect very small finite volume effects (Takahashi et al, 2008). We want to remark that the results presented in this paper are consistent with those derived using the  $1296 \text{ h}^{-1}\text{Mpc}$  and  $162 \text{ h}^{-1}\text{Mpc}$  simulations boxes, thus reinforcing our conclusions.

The nine simulations that we have performed have a very large resolution compared to that of previous studies on structure formation in dark energy cosmologies. Each simulation contains  $512^3$  particles,  $512^3$  grids elements on the coarse level with 6 – 7 additional refinement levels. Each simulation required about 20.000 hours of computation on 64 processors, while the more structured simulations demanded 300 hours of elapsed time.

Table 3 summarizes the characteristics of the simulations for each of the three cosmological models.

### 5.4 Numerical results

A visual summary of the N-body simulations is shown in Figure 7, where we plot for each cosmology the projected dark matter density on the  $x - y$  plane at  $z = 0$  from the simulations of box length  $162 \text{ h}^{-1}\text{Mpc}$  (panels from top to bottom correspond to  $\Lambda$ CDM, SUCDM and RPCDM respectively) at scales  $162 \text{ h}^{-1}\text{Mpc}$  (first column panels),  $32 \text{ h}^{-1}\text{Mpc}$  (second column panels) and  $6 \text{ h}^{-1}\text{Mpc}$  (third column panels). We may notice the high spatial resolution of these simulations which probe both cosmological scales, filaments, halos and even the inner profile of dark matter halos.

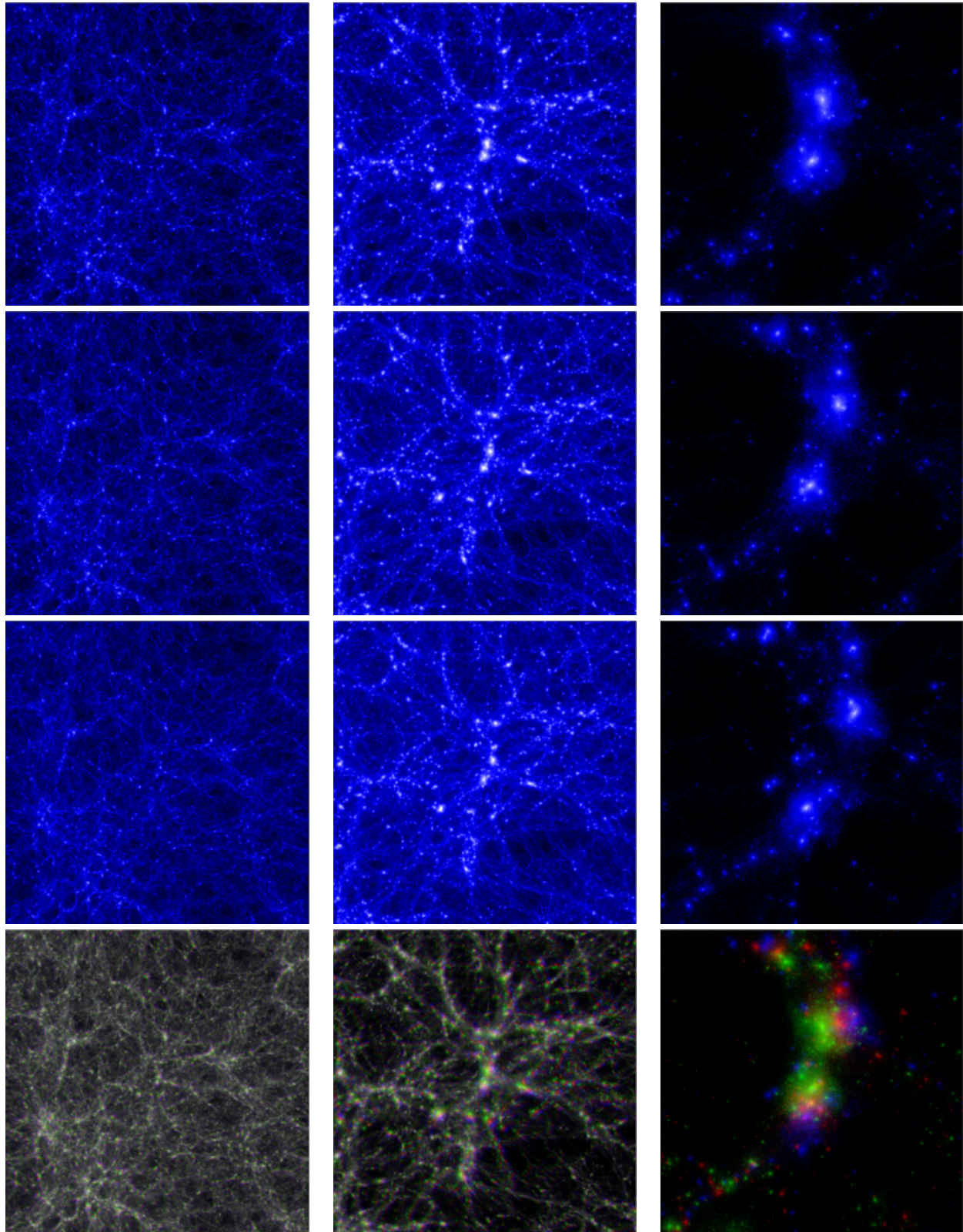


**Figure 7.** Projections of the DM density fields for the  $\Lambda$ CDM (first line), SUCDM (second line) and RPCDM (third line). Left panels correspond to one full simulation box of  $162 \text{ h}^{-1}\text{Mpc}$  length projected on the x-y plane, central and right panels respectively illustrate a cube of  $32 \text{ h}^{-1}\text{Mpc}$  and  $6 \text{ h}^{-1}\text{Mpc}$  lengths extracted from the full simulation ( $162 \text{ h}^{-1}\text{Mpc}$ ) and then projected on their x-y plane. The color levels then indicate the surface density of these projections (in units of the cosmological mean surface density) with ranges  $[2.03 \times 10^{-1}; 6.41 \times 10^1]$ ,  $[2.63; 8.32 \times 10^2]$ ,  $[6.33 \times 10^1; 1.26 \times 10^4]$  for the boxes of  $162 \text{ h}^{-1}\text{Mpc}$  (left),  $32 \text{ h}^{-1}\text{Mpc}$  (center),  $6 \text{ h}^{-1}\text{Mpc}$  (right) respectively. The last three panels in the bottom line show the superposition of the DM density field for the three different cosmologies with color encoding: green ( $\Lambda$ CDM), red (SUCDM) and blue (RPCDM). On large scales, the differences are small (black and white regions), while on small scales these are clearly obvious (multi-color region).

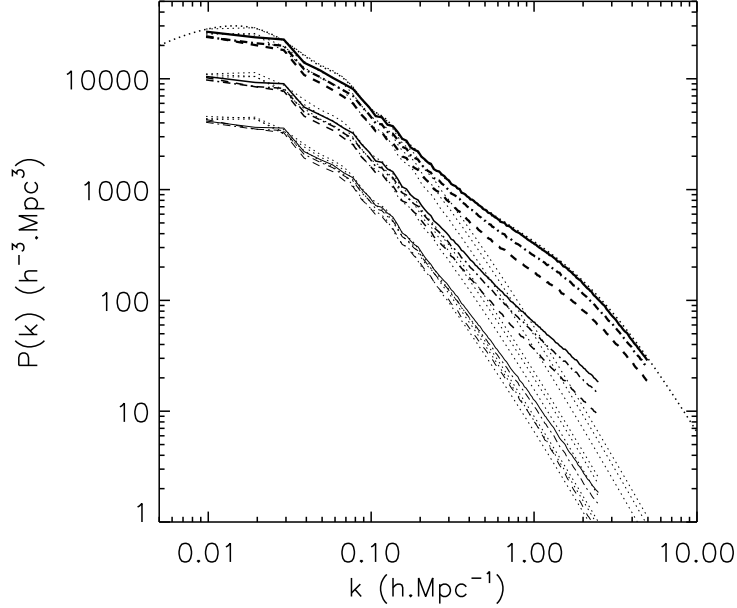


**Figure 8.** Comparison between linear (dot lines) and non-linear power spectra from the N-body simulations with box length of  $648 h^{-1} \text{Mpc}$  for the different cosmologies ( $\Lambda\text{CDM}$ : solid line;  $\text{RPCDM}$ : dash line;  $\text{SUCDM}$ : dash-dot line) at three different epochs (from bottom to top:  $a = 0.3, 0.5, 1$ ). For comparison we plot the Smith et al. (2003) predictions of the power spectrum at  $z=0$  for the  $\Lambda\text{CDM}$  cosmology (top dotted line).

In the images we have kept the same color intensity coding which facilitates a visual appreciation of the differences of the clustering process for the different cosmologies. As already found by Füzfa and Alimi (2006), realistic quintessence cosmologies yield a DM density field that is less structured than that of the concordance  $\Lambda\text{CDM}$ , especially on small scales. The visible features of the density field also show that DM structures have undergone a different evolution in terms of collapse and merging history. For instance this can be seen by comparing the DM density distribution of the three models in the zoomed images at  $6 h^{-1} \text{Mpc}$ . Such differences are emphasized in the bottom panels of Figure 7 where we plot in different colors (while keeping fixed the coding of the color intensity with the density field) the superposition of the DM density field of the three cosmologies: green ( $\Lambda\text{CDM}$ ), red ( $\text{SUCDM}$ ) and blue ( $\text{RPCDM}$ ). The white regions correspond to an exact surposition of the primary colors, thus indicating regions which have undergone similar clustering. From the panels in the top row we can see that on the large scales the DM clustering is nearly similar for the three different models, since it is dominated by a white color. In contrast, when zooming on smaller scales we can see the emergence of the individual color associated with the density field of each model. In particular we may notice that the DM structures are modified in shape, size and location.

In order to quantify such differences for each simulation box we measure the matter power spectrum using the POWMES code<sup>6</sup> described in great detail in Colombi et al. (2009). This code relies on a Taylor expansion of the trigonometric functions and turns out to provide a very accurate estimation of power spectra for N-body experiments. For all snapshots, we have used an expansion of order 3, with a grid of size  $256^3$ , a number of foldings of 3 (to probe high wavenumbers) without subtraction of the shot noise (since in this paper we mainly focus on ratios of power spectra). For the range of wavenumbers considered, the errors in the power spectrum estimation are negligible compared to the approximations of the N-body solver.

The measured non-linear power spectra in the simulations of box length  $648 h^{-1} \text{Mpc}$  are plotted in Figure 8 for redshifts  $z = 0, 1$  and  $2.3$  (i.e.  $a = 1, 0.5$  and  $0.3$ ). For comparison we also plot the corresponding linear power spectra evolved backward using the homogeneous growth function as described in Section 4. To be conservative we restrict ourselves to wavenumber below the Nyquist frequency, which is given by our maximum resolution at a given redshift divided by a chosen value of 32. In this way, our highest wavenumber is of order of one or two times the Nyquist frequency associated to the coarse grid. According to the cosmic code comparison analysis by Heitmann et al. (2005, 2008), the majority of the tested N-body codes agree at 5% level on scales which are below twice the Nyquist frequency of the coarse grid. However, above four times this frequency the agreement becomes worse and deviations can be larger than ten percent, this is why we choose the more conservative criterion described above. Moreover, we focus on the power spectrum below  $k = 5 h \text{Mpc}^{-1}$  since at  $z = 0$  the baryon contribution is of a few percents at this scale and increases up to 10 percents at  $k = 10 h \text{Mpc}^{-1}$  (Jing et al, 2006). We note that

<sup>6</sup> We thank Stephane Colombi for kindly providing us with the code.



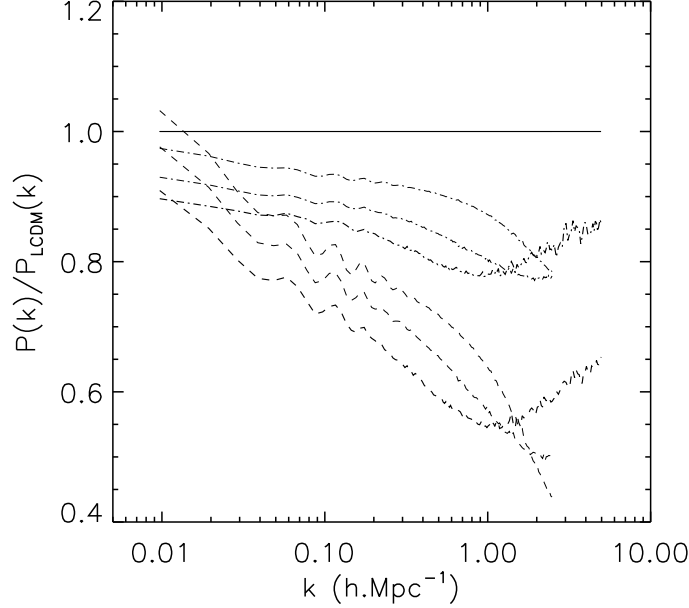


**Figure 9.** Evolution of the non-linear matter power spectrum in quintessence cosmologies relative to the  $\Lambda$ CDM case (RPCDM: dash line; SUCDM: dash-dot line). From top to bottom:  $a = 0.3, 0.5, 1$ , the thickness of the curves is proportional to the scale factor.

these uncertainties only concern the absolute prediction of the power spectrum and not the ratio of power spectrum which we will describe in Section 5.5.

Overall quintessence models possess less power than  $\Lambda$ CDM, which confirms the expectation of the linear analysis. Again this can be interpreted as a consequence of the fact that a record of dark energy during the linear collapse is kept through the non-linear regime. We may notice several important features. Firstly, the amplitude of the bumps on the large scales grows earlier in  $\Lambda$ CDM, since the large scales in the simulation boxes evolve nearly linearly, then this result is consistent with the model differences expected from the linear growth factor discussed in Section 4. Secondly, we can see that at small scales the departure from linearity occurs earlier in  $\Lambda$ CDM than in quintessence models. Again this is consistent with the fact that during the matter dominated era the concordance model decelerates more efficiently than quintessence cosmologies (see also bottom panel of Figure 2), causing a faster rate of gravitational infall of dark matter, thus entering in the non-linear regime at earlier times.

One last point concerns the detectability of such differences through measurements of the galaxy power spectrum. On the large scales the measured power spectra matches the linear predictions which we have shown to be in agreement with SDSS data provided the large scale galaxy bias parameter assumes slightly different values for each realistic cosmology. In order to detect the imprint of dark energy on the non-linear scale of the galaxy power spectrum is therefore necessary to have an accurate knowledge of the galaxy bias on those scales. In such a case measurements of the weak lensing power spectrum probing the gravitating mass distribution can be more reliable (see e.g. Huterer 2002). In the upcoming years several weak lensing surveys will provide accurate tomographic measurements of the shear power spectrum which can be especially sensitive to the dark energy imprint on the small scales distribution of dark matter halos (Ivezic et al. 2008).

## 5.5 Imprints of dark energy on cosmic structure formation

In this section, we aim to provide a detailed physical understanding of the imprint of the three realistic models on the non-linear power spectrum. For this reason rather than focusing on the power spectrum of each model we focus on their ratios. This has also an advantage from a purely numerical point of view, since McDonald et al. (2006) have investigate the sensitivity of power spectra to changes of the starting redshift, box size, mass resolution, force resolution and time step size and shown that most of the errors cancel out when considering ratios of power spectra, with an expected precision of a few percents around the Nyquist frequency of the coarse grid.

In Figure 9 we plot the ratio of the measured non-linear power spectrum of the RPCDM (dash line) and SUCDM (dash-dot line) to that of the concordance  $\Lambda$ CDM,  $r = P_{nl}^{QCDM}(k)/P_{nl}^{\Lambda CDM}(k)$ . All quintessence cosmologies are characterized by  $r < 1$ , corresponding to a smaller amount of clustering with respect to  $\Lambda$ CDM. We may notice that the discrepancy with respect to the concordance model is not uniform, since it varies with scale, redshift and quintessence model. Overall the RPCDM differs from the  $\Lambda$ CDM more than the SUCDM, with a maximum

discrepancy of about 40% for the RPCDM and about 20% for the SUCDM. Besides in both quintessence cosmologies  $r$  decreases as function of  $k$  in the interval  $0.01 \text{ h Mpc}^{-1} \lesssim k \lesssim 1 \text{ h Mpc}^{-1}$ , and increases at smaller scales,  $k > 1 \text{ h Mpc}^{-1}$ .

This is consistent with the fact that on the large scales the linear growth rate is suppressed with respect to the  $\Lambda$ CDM case more in the RPCDM than SUCDM (see Fig. 3). On the other hand the small scales are affected by non-linear processes which increases the amount of clustering, thus inverting the trend. We can also notice that as consequence of the non-linear collapse at a given time there exists a characteristic non-linear scale (corresponding to the minimum of the  $r$ -curves) below which the DM clustering increases as function of  $k$ . Such a scale shifts from the right to the left (from  $k \approx 1 \text{ h Mpc}^{-1}$  to  $\approx 3 \text{ h Mpc}^{-1}$ ) for increasing redshift, i.e. the smaller the scale the earlier it enters in the non-linear regime. Furthermore, the amount of clustering on the non-linear scales in the RPCDM model differs from the SUCDM case, thus indicating a characteristic imprint of the nature of DE.

In order to isolate the non-linear contributions and remove the linear effects we compute the ratio:

$$R_{\text{QCDM}} = \frac{P_{nl}^{\text{QCDM}}(k) P_{lin}^{\Lambda\text{CDM}}(k)}{P_{nl}^{\Lambda\text{CDM}}(k) P_{lin}^{\text{QCDM}}(k)}, \quad (18)$$

which is shown in Figure 10 for  $a = 1, 0.5$  and  $0.3$  respectively. We can see that all scales corresponding to  $k \lesssim 0.1 - 0.2 \text{ h Mpc}^{-1}$  are in the linear regime, since  $R_{\text{QCDM}} \approx 1$  (within 1 – 2% accuracy). On smaller scales corresponding to  $0.1 \text{ h Mpc}^{-1} \lesssim k \lesssim 1 \text{ h Mpc}^{-1}$ , the ratio decreases for both quintessence models with respect to the  $\Lambda$ CDM case, as already seen in Figure 9. This suggests that also non-linear effects contribute to the power suppression that characterizes quintessence models. This corresponds to the quasi-linear regime. On the other hand on scales which are below the same corresponding to the location of the minimum of the  $R_{\text{QCDM}}$  function,  $k \approx 1 \text{ h Mpc}^{-1}$ , the non-linear clustering of DM in quintessence models increases very rapidly, eventually exceeding that of the  $\Lambda$ CDM ( $R_{\text{QCDM}} > 1$ ). In other words as time elapses the non-linear growth of structure becomes more and more efficient in QCDM models than in  $\Lambda$ CDM, with the RPCDM having a larger growth than the SUCDM. This can be understood in terms of the stable clustering regime characterizing these scales (Hamilton et al. 1991) or alternatively to the halo term (Smith et al. 2003), such that the growth of the power spectrum tends to slow down once the structures become more and more virialised.

At this point, we have isolated three main contributions to the rough differences between the power spectra of different dynamical dark energy models. On linear scales ( $k < 0.1 \text{ h Mpc}^{-1}$ ) the discrepancies can be explained by the differences in the linear power spectra (which are due to the various cosmological parameters needed to reproduce the CMB and SNIa, the spatial fluctuations of the quintessence as well as the different background evolutions). On quasi-linear scales ( $0.1 \text{ h Mpc}^{-1} < k < 1 \text{ h Mpc}^{-1}$ ), the discrepancies can be mainly explained by the non-linear amplification of the growth rate. Since the linear amplitude is different, a given mode enters the non-linear regime at a different time. On the halo scales ( $k > 1 \text{ h Mpc}^{-1}$ ), the differences are roughly due to the saturation of the growth of structures as they start to be virialised. Again, this halo term depends mainly on the amplitude of the linear growth rate.

All the effects described above are rather well accounted for by the Smith et al. (2003) fitting function of the matter power spectrum. In order to check whether there are additional non-linear contributions to the final shape of the power spectrum, we compute the ratio

$$RS_{\text{QCDM}} = \frac{P_{nl}^{\text{QCDM}}(k) P_{Smith}^{\Lambda\text{CDM}}(k)}{P_{nl}^{\Lambda\text{CDM}}(k) P_{Smith}^{\text{QCDM}}(k)}, \quad (19)$$

plotted in Figure 11 (top panel) for  $z = 0$ . We can see that on scales  $k > 1 \text{ h Mpc}^{-1}$  (halo scale) there is an enhancement of the power in quintessence models compared to the Smith et al. (2003) prediction. This can be as large as 5% at  $k = 5 \text{ h Mpc}^{-1}$  and reach even larger values at higher wavenumbers. This deviation is not a numerical artifact because as we already mentioned above, these wavenumbers are below the Nyquist frequency. Moreover the ratio of power spectra between two models is less sensitive to numerical errors than the absolute power spectrum itself, as previously mentioned.

This result is qualitatively consistent with a number of works (McDonald et al. 2006; Ma 2007; Francis et al. 2007 and Casarini et al. 2009). For instance, in Figure 11 we plot the deviations for SUCDM (dash-dotted line) and RPCDM models and for comparison those tabulated by McDonald et al. (2006) (thin continuous lines) in the case of dark energy models parametrized by constant equation of state  $w = w_0$  (see table 2 for the values of  $w_0$ ). We find that deviations are nearly of the same order, 5% level, towards higher values of the power spectrum at large  $k$ . Nonetheless there are some important differences. First of all, the deviations appear to be stronger in dynamical quintessence models than in the  $w = \text{const.}$  case. Secondly, the shape is slightly different near  $k = 5 \text{ h Mpc}^{-1}$ . Finally, the disagreement is stronger for the SUCDM cosmology. The reason is rather obvious if we look at Fig. 2 (top panel). In fact the time variation of the equation of state is larger in SUCDM. Recently, a more sophisticated way of fitting these deviations has been proposed for a linear parametrization of the equation of state (Francis et al. 2007) and extended to quintessence models (Casarini et al. 2009). The idea is to use the prediction of McDonald et al. (2006) for an effective constant eos  $w_{eff}$ , that predicts the same distance to the last scattering surface of a dynamical quintessence model. Although interesting, the generality of this approach is not clear. In addition, the mapping between the quintessence model and the effective description with constant eos at different epochs is not straightforward to implement, and can easily lead to misinterpretations. In comparison, the complete approach described here is physically well motivated and allows for a robust accounting of the various effects. As

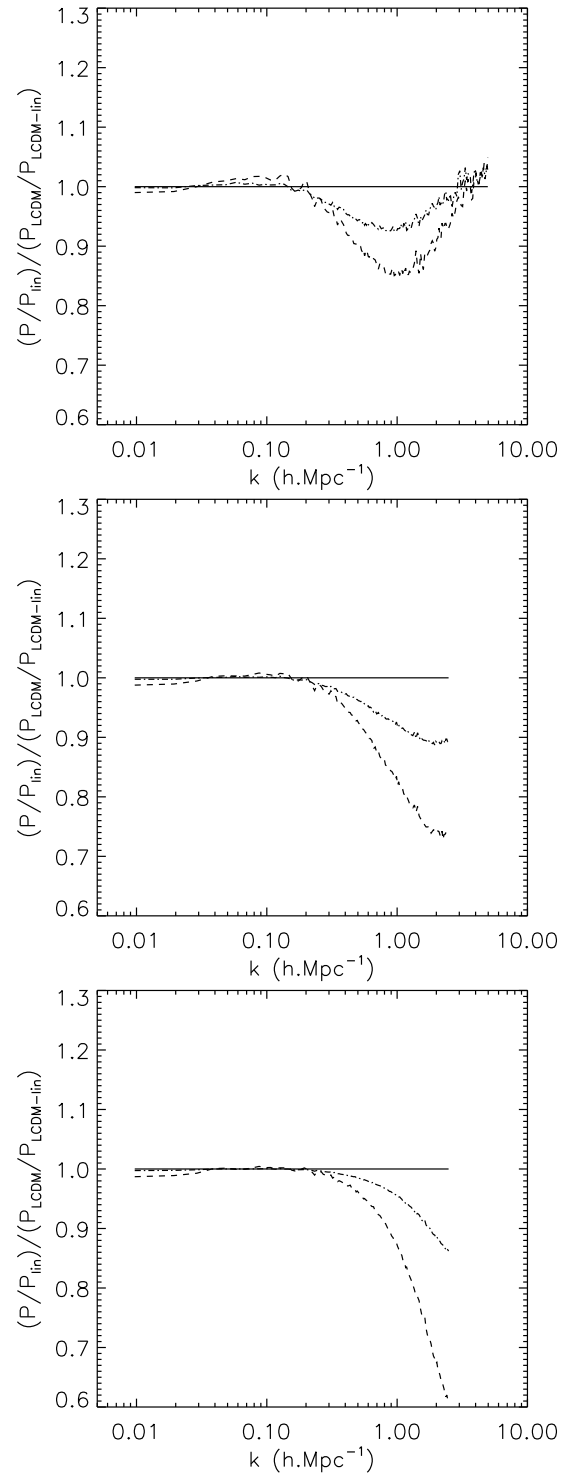


**Figure 10.** Ratio of the non-linear power spectrum relative to linear predictions for the different cosmologies as a measurement of the evolution of non-linearity in the gravitational collapse. Panels from top to bottom corresponds to  $a = 1, 0.5, 0.3$  ( $\Lambda$ CDM: straight line; RPCDM: dashed line; SUCDM: dash-dotted line).

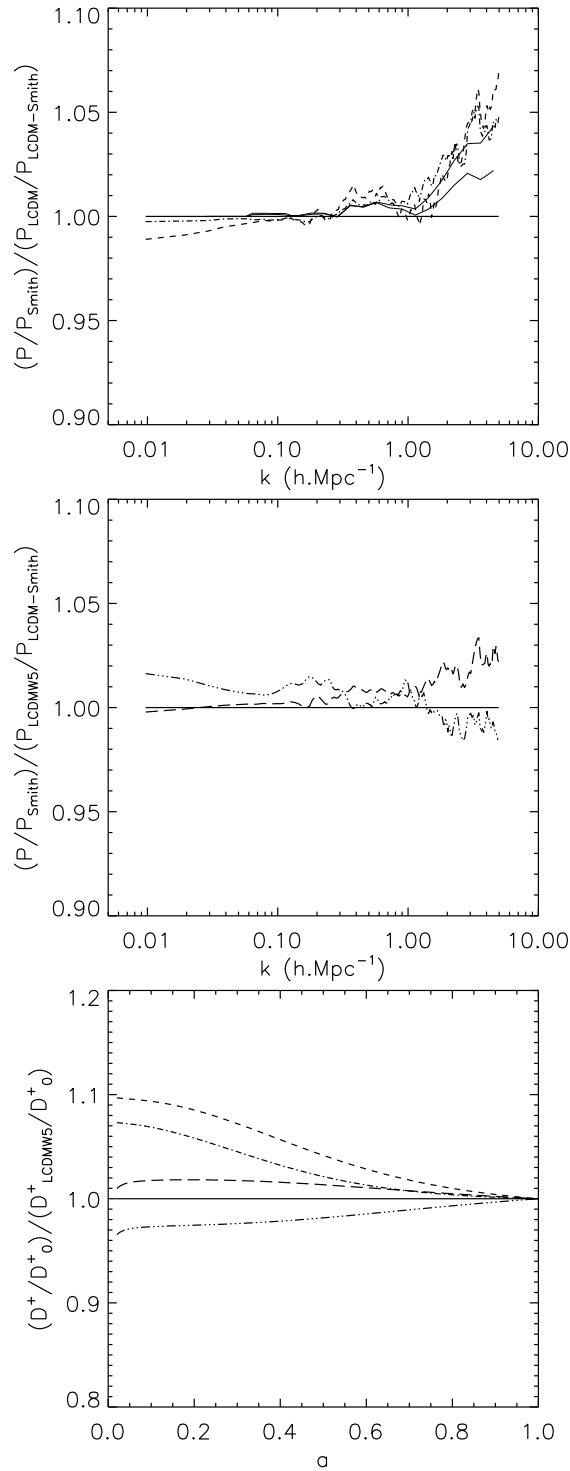


**Figure 11.** Top panel: Ratio of the non-linear power spectrum normalized to Smith et al. (2003) fit for RPCDM (dashed) and SUCDM (dot-dashed) relative to the  $\Lambda$ CDM. The thin continuous line are the constant eos expectation for RPCDM (top) and SUCDM (bottom). Middle pane: as in the top panel but for the  $\Lambda$ CDM WMAP I (triple dot-dashed line) and  $\Lambda$ CDM WMAP III (long dashed line) models. Bottom panel: Linear growth factor relative to the  $\Lambda$ CDM WMAP5 one. The deviations at high  $k$  of the power spectra are correlated with the linear growth histories.

we have shown here, each dark energy model has a specific cosmological evolution which leads to specific imprints, and it is not clear how well these features can be precisely accounted for in the approach proposed by Casarini et al. (2009).

This point is also related to another important aspect, namely the universality of fitting procedures of the non-linear power spectrum based on large numerical simulations. As already pointed out by Ma (2007), the history of structure formation is not properly taken into account by standard predictions such as that provided by Smith et al. (2003) or Peacock & Dodds (1996). This is because the non-linear power spectrum is expressed as a fitting function of the cosmological parameters and the linear power spectrum. To some extent these fitting functions can be considered as instantaneous predictions from the linear power spectrum, since they do not depend in any way on the past evolutionary history of the structure formation of the model specified by the set of cosmological parameters. However, the non-linear regime should in principle have a fossil record of such history and thus the past influence of dark energy. As an example Ma (2007) has shown that the deviations from one model to another scale as their relative linear growth histories. Indeed, the imprint of the past evolution on the non-linear power spectrum is also present in the case of the realistic models considered here. In order to emphasize this result we have run two additional  $\Lambda$ CDM simulations for comparison: LCDMW1 (WMAPI cosmological parameters:  $\Omega_m = 0.29$ ,  $\Omega_\Lambda = 0.71$ ,  $\Omega_b = 0.047$ ,  $h = 0.72$ ,  $\sigma_8 = 0.9$  and  $n_s = 0.99$ ) and LCDMW3 (WMAPIII cosmological parameters:  $\Omega_m = 0.24$ ,  $\Omega_\Lambda = 0.76$ ,  $\Omega_b = 0.042$ ,  $h = 0.73$ ,  $\sigma_8 = 0.74$  and  $n_s = 0.951$ ). The deviations with the respect to the Smith et al. (2003) prediction are shown in Figure 11 (middle panel). We may note that the curves are in remarkably good agreement, although some small deviations (below 5%) are present. The different level of deviations between the realistic quintessence models and these  $\Lambda$ CDM test runs can be explained in terms of their past history as described by the linear growth factor evolution. In Figure 11 (bottom panel) we plot the linear growth factor as function of the scale factor relative to the  $\Lambda$ CDM WMAP5 case. We can see that deviations with respect to Smith et al. (2003) at high  $k$  are well correlated to the maximum deviations between the linear growth histories of the different models. Thus indicating that the past history of cosmic structure formation plays an important role since the features introduced in the matter power spectrum are not erased by the non-linear collapse: the non-linear collapse contributes to the specific imprints of the DE model. A semi-analytical implementation of the structure formation history on the calculation of the non-linear power spectrum can be obtained using the halo model (Cooray & Sheth 2002), which accounts for the instant of collapse, the overdensity at virialization and the concentration parameters which depends on the assembly history (Wechsler et al. 2002). This is further motivation for us to study in great details the impact of dark energy on the mass function and on the internal structure of dark matter halos, which will be discussed in other articles of the series.

## 6 CONCLUSIONS

In this paper, we have studied the imprint of quintessence on the non-linear clustering of dark matter halos through state-of-the-art N-body simulations. To this purpose we have focused on two scalar field models specified by Ratra-Peebles and SUGRA potentials. Upon these models we have performed a series of high resolution N-body simulations and shown that quintessence leaves a distinctive signature on the structure formation at all scales and especially during the non-linear regime. This is in contrast with conclusions drawn from previous works in the literature. Some of these studies limited their analysis to dark energy models parametrized by a simply constant or linearly varying equation of state, which fail to grasp the specific feature of dark energy clustering throughout the cosmological evolution. Other analysis have focused on the same class of quintessence models; nevertheless, in all these studies the cosmological parameters were set to values corresponding to the concordance  $\Lambda$ CDM model, thus missing crucial features which are necessary to fully evaluate the impact of dark energy on the structure formation.

The benchmark of dark energy models considered has been selected through a likelihood data analysis which we performed to determine quintessence model parameters that fit CMB and SN Ia data within  $2\sigma$  significance from the  $\Lambda$ CDM scenario. These models are statistically indistinguishable from the concordance model; nevertheless they are characterized by different cosmic expansion histories, which in addition to the effect of dark energy perturbations modify the growth of the linear dark matter perturbations, thus leaving quintessence model dependent signatures on the linear matter power spectrum. These imprints are consistent with current measurements of the galaxy power spectrum from SDSS data, and statistically indistinguishable with the respect to the  $\Lambda$ CDM model.

The results of the N-body simulations clearly show that the model dependent features present at the homogeneous and linear perturbation level are amplified by the non-linear collapse of dark matter structures. We find that quintessence affects the non-linear matter power spectrum at all scales, with a suppression of power at the small scales compared to the  $\Lambda$ CDM case. However when the effects of the different linear evolution histories are taken into account, the non-linear clustering of DM appears to be more efficient in quintessence cosmologies than in the standard  $\Lambda$ CDM scenario. These features can only be partly understood in the Smith et al. (2003) phenomenology framework, that as we have shown here it needs to be complemented with the full cosmic structure formation history to account for the imprint of DE on the non-linear matter power spectrum. This support the idea that a robust evaluation of the impact of DE on the non-linear structure formation requires an accurate and self-consistent implementation of the quintessence model in the N-body simulations.

The imprints of quintessence on the DM distribution that we obtained here would affect the gas on all scales. As the gas collapses inside DM potential wells, the gas distribution would also keep a record of the nature of DE. On large scales, the gas distribution tracks the DM

one while on small scales the gas cooling accelerates the gas collapse but not the DM one. As a result, the star formation rate (SFR) could be affected by DE. From the results of this paper, the SFR is expected to be smaller in quintessential universes than in the  $\Lambda$ CDM model due to the smaller  $\sigma_8$  in the first. However, the SFR in the past could be more important compared to the SFR today when DE is quintessence rather than  $\Lambda$ . This is because the ratio  $D_+/D_+(a_0)$  in quintessence models is higher than in  $\Lambda$ CDM. As well, the SFR at  $z = 0$  in quintessence models should be different than the one of a  $\Lambda$ CDM model with the same value of  $\sigma_8$ . The history of SFR is therefore expected to keep a specific record of the cosmic expansion history and therefore of the nature of DE. More precisely, it has been shown by Rasera & Teysier (2006) that the total SFR in the Universe is ruled at first order by the amount of DM halos with total mass higher than a critical Jeans-like mass called the filtering mass. This prescription could allow one to deduce SFR from DM halo mass function (see the sequel of this paper). In addition, another expected imprint of DE on the gas would arise from the gas collapse itself whose details, like accretion, cooling, SFR, supernovae feedback, ..., depend on the cosmic expansion history. Finally, the feedback of the gas on DM will slightly affect DM distribution on small scales (see also Guillet et al., 2009).

In this work, we focused on the DE signature on the non-linear matter power spectrum, in a series of upcoming papers we will present other characteristic imprints of dark energy scenarios on the non-linear structure formation, in particular we will provide a detailed study of the halo mass functions and the physical properties of dark matter halos. The results of our analysis already suggest that, contrary to common belief, an accurate comparison between the small and large scale distribution of matter in the Universe can in principle shed light on the nature of dark energy.

## ACKNOWLEDGEMENTS

Numerical simulations for parameter selection were made at the UCLouvain HPC Center (Belgium) under project FRFC 2.4502.05, and on the local computing resources at LUTH (Observatoire de Paris, France) and Unité de Systèmes Dynamiques (FUNDP, Belgium). This work was granted access to the HPC resources of CCRT under the allocation 2009-t20080412191 made by GENCI (Grand Equipement National de Calcul Intensif). We would like to thank Romain Teysier, Stéphane Colombi and Simon Prunet for their valuable advices concerning the RAMSES, POWMES and MPGRAFIC softwares. This work was supported by the Horizon Project ([www.projet-horizon.fr](http://www.projet-horizon.fr)). A.F. is supported by the Belgian "Fonds de la Recherche Scientifique" (F.N.R.S. Postdoctoral Researcher) and is associated researcher at CP3 (UCL, Belgium) and LUTH, Observatory of Paris. V.B. is supported by the Belgian Federal Office for Scientific, Technical and Cultural Affairs through the Interuniversity Attraction Pole P6/11.

## REFERENCES

- Amendola L., 2000, Phys. Rev. D, 62, 043511  
 Aghanim N., da Silva A. & Nunes N. J., 2009, Astron. Astrophys, 496, 637  
 Alimi J.-M., Füzfa A., 2008, J. Cosmology Astroparticle Phys., 09, 014  
 Allen S.W., Schmidt R.W. & Fabian A.C., 2002, MNRAS, 334, L11  
 Astier P. et al., 2006, Astron. Astrophys., 447, 31-48  
 Baccigalupi, C. et al., 2002, Phys. Rev. D, 65, 063520  
 Benabed K. & Bernardeau F., 2001, Phys. Rev. D, 64, 083501  
 Bennett C.L. et al., 2003, ApJ Suppl., 148, 39  
 Bertschinger E., 1995, arXiv:astro-ph/9506070v1  
 Bertschinger E., 2001, ApJS, 137, 1  
 Bode P. et al., 2001, ApJ, 551, 15-22  
 Binetruy P., 1999, Phys. Rev. D, 60, 063502  
 Brax P. & Martin J., 2000, Phys. Rev. D, 61, 103502  
 Brax P., Martin J. & Riazuelo A., 2000, Phys. Rev. D, 62, 103505  
 Cabre A. et al., 2006, MNRAS, 372, L23  
 Caldwell R.R., Dave R. & Steinhardt P.J., 1998, Phys. Rev. Lett., 80, 1582  
 Capozziello S., Cardone V.F. & Troisi A., 2005, Phys. Rev. D, 71, 043503  
 Caresia P., Matarrese S. & Moscardini L., 2004, ApJ, 605, 21  
 Casarini L., Macciò A. V. & Bonometto S. A., 2009, Journal of Cosmology and Astro-Particle Physics, 3, 14  
 Chevallier M. & Polarski D., 2001, Int. J. Mod. Phys. D, 10, 213  
 Cole S. et al., 2005, MNRAS, 362, 505  
 Colombi S. et al., 2009, MNRAS, 393, 511  
 Colombo L.P.L. & Gervasi M., 2006, J. Cosmology Astroparticle Phys., 10, 001  
 Copeland E.J., Sami M. & Tsujikawa S., 2006, Int.J.Mod.Phys. D, 15, 1753  
 Corasaniti P.S. & Copeland E.J., 2002, Phys. Rev. D, 65, 043004  
 Corasaniti P.S. et al., 2003, Phys. Rev. Lett., 90, 091303  
 Corasaniti P.S. et al., 2004, Phys. Rev. D, 70, 083006

- Cooray A., & Sheth R., 2002, *Physics Report*, 372, 1
- Crocce M., Pueblas S., & Scoccimarro, R., 2006, *MNRAS*, 373, 369
- Dave R., Caldwell R.R. & Steinhardt P.J., 2002, *Phys. Rev. D*, 66, 023516
- De Bernardis P. et al., 2000, *Nature*, 404, 955
- Di Pietro E. & Claeskens J.-F., 2003, *MNRAS*, 341, 1299
- Dolag K. et al., 2004, *Astron. Astrophys.*, 416, 853-864
- Dvali G.R., Gabadadze G. & Porrati M., 2000, *Phys. Lett. B*, 485, 208
- Efstathiou G. et al., 2002, *MNRAS*, 330, L29
- Eisenstein D.J. et al., 2005, *ApJ*, 633, 560
- Francis M. J., Lewis G. F. & Linder E. V., 2007, *MNRAS*, 380, 1079
- Füzfa A. & Alimi J.-M., 2006, *AIP Conf.Proc.*, 861, p.858, American Institute of Physics, New-York, USA
- Giannantonio T. et al., 2008, *Phys. Rev. D*, 77, 123520
- Guillet T., Teyssier R. & Colombi S., 2009, arXiv:0905.2615v2 [astro-ph.CO]
- Guzzo L. et al., 2008, *Nature* 451, 541
- Hamilton A. J. S. et al., 1991, *ApJL*, 374, L1
- Heitmann K. et al., 2005, *ApJS*, 160, 28
- Heitmann K. et al., 2008, *Computational Science and Discovery*, 1, 015003
- Huterer D., 2002, *Phys. Rev. D*, 65, 063001
- Ivezic Z. et al., 2008, arXiv:0805.2366v1 [astro-ph]
- Jing Y. P. et al., 2006, *ApJL*, 640, L119
- Khoury J. & Weltman A., 2004, *Phys. Rev. D*, 69, 044026
- Klypin A. et al., 2003, *ApJ*, 599, 31
- Knop R.A. et al., 2003, *ApJ*, 598, 102
- Komatsu E. et al., 2009, *ApJS*, 180, 330
- Kowalski M. et al., 2008, *ApJ*, 686, 749
- Kunz M. et al., 2004, *Phys. Rev. D*, 70, 041301
- La Vacca G. et al., 2009, *J. Cosmology Astroparticle Phys.*, 04, 007
- Lewis A., Challinor & A., Lasenby A., 2000, *ApJ*, 538, 473
- Lewis A. & Bridle S., 2002, *Phys. Rev. D*, 66, 103511
- Lewis A. & Weller J., 2003, *MNRAS*, 373, 561
- Linder E.V., 2003, *Phys. Rev. Lett.*, 90, 091301
- Lokas E.L., Bode P. & Hoffman Y., 2004, *MNRAS*, 349, 595
- Ma C.P. et al., 1999, *ApJ*, 521, L1
- Ma Z., 2007, *ApJ*, 665, 887
- Maio U. et al., 2006, *MNRAS*, 373, 869
- Masiero A., Pietroni M. & Rosati F., 2000, *Phys. Rev. D*, 61, 023504
- McEwen J. D. et al., 2008, *MNRAS* 384, 1289
- McDonald P., Trac H. & Contaldi C., 2006, *MNRAS*, 366, 547
- Mohayaee R. & Tully R. B., 2005, *ApJ*, 635, L113
- Munshi D., Porciani C. & Wang Y., 2004, *MNRAS*, 349, 281
- Peacock J. A. & Dodds S. J., 1996, *MNRAS*, 280, L19
- Peebles P.J.E., 1993, *Principles of Physical Cosmology*, Princeton University Press
- Perlmutter S. et al., 1999, *ApJ* 517, 565
- Perrota F. & Baccigalupi C., 1999, *Phys. Rev. D*, 59, 123508
- Prunet S. et al., 2008, *ApJS*, 178, 179
- Rasera Y. & Teyssier R., 2006, *Astron. Astrophys*, 445, 1
- Ratra B. & Peebles P.J.E., 1998, *Phys. Rev. D*, 37, 3406
- Riess A.G. et al., 1998, *Astron. J.*, 116, 1009
- Riess A.G. et al., 2001, *ApJ*, 560, 49
- Riess A.G. et al., 2007, *ApJ*, 659, 98
- Schimdt C. et al., 2007, *Astron. Astrophys*, 463, 405
- Smith R. E. et al., 2003, *MNRAS* , 341, 1311
- Solevi P. et al., 2006, *MNRAS*, 366, 1346
- Spergel D.N. et al., 2003, *ApJS*, 148, 175
- Spergel D.N. et al., 2007, *ApJS*, 170, 377
- Steinhardt P.J., Wang L. & Zlatev I., 1999, *Phys.Rev. D*, 59, 123504
- Takahashi R. et al., 2008, *MNRAS*, 389, 1675
- Tegmark M. et al., 2004, *Phys. Rev. D*, 69, 103501
- Tegmark M. et al., 2006, *Phys. Rev. D*, 74, 123507
- Teyssier R., 2002, *Astron. Astrophys*, 385, 337
- Viana P. & Liddle A.R., 1998, *Phys. Rev. D*, 57, 674
- Wechsler, R. H. et al., 2002, *ApJ*, 568, 52
- Weinberg S., 1989, *Rev. Mod. Phys.*, 61, 1
- Wetterich C., 1988, *Nucl. Phys. B*, 302, 668

